

# Geochemistry and petrogenesis of some gabbroic intrusions invaded the basement rocks from Al-Maqatirah and Al-Ahkum areas, SE Taiz, Republic of Yemen

Mukhtar A. Nasher \*, Hussein A. Sultan and Abdul-Hamid Malek

Department of Geology, Faculty of Applied Sciences, University of Taiz, Taiz, Yemen

\*Corresponding author: [mukhtar\\_nasher@yahoo.com](mailto:mukhtar_nasher@yahoo.com)

## ABSTRACT

The Al-Maqatirah and Al-Ahkum areas are located in SE of Taiz within the southwestern outcrops of the basement rocks of Yemen, which represent the southern extension of the Arabian Nubian Shield (ANS). This paper focuses on the study of gabbroic intrusions that have invaded these basement rocks in these areas.

These gabbroic intrusions were unmetamorphosed, variably altered, and sometimes affected by Na-rich fluid fluxes. They exhibit many types of textures and structures, and according to the abundance and appearance of major mineral constituents, these gabbroic rocks are classified into several types. Chemically, these gabbroic intrusions are classified as low-Ti intrusions generated from low-Ti magma, which is characteristic of an intra-oceanic island arc setting and formed in a subduction zone setting by partial melting and re-melting of a depleted peridotite mantle source. However, some samples show indications of subsurface mixing of contemporaneous magma batches with low Ti and high Ti compositions. The major element compositions of these gabbroic rocks reflect their derivation from primitive magma subjected to significant degrees of fractional crystallization.

These gabbroic intrusions have an ocean island basalt (OIB) signature and transitional character of magma from alkaline to sub-alkaline (tholeiitic) magma series, which indicate their derivation by variable degrees of partial melting of the mantle source at various depths during the change from arc to intraplate setting. The OIB signature of these mafic intrusions suggests lithospheric attenuation and significant upwelling of the asthenosphere caused by continental rifting, which mostly occurs during the formation of the Arabian lithosphere. Finally, the studied gabbroic intrusions can be compared with similar gabbroic intrusions in the Arabian-Nubian shield from Saudi Arabia, which are emplaced post-collision at the end of the Pan-African Orogeny and generated from mafic magma derived from a peridotite mantle source.

## ARTICLE INFO

### Keywords:

petrogenesis, geochemistry, gabbroic intrusions, basement rocks, Al Maqatirah, Al-Ahkum areas, Taiz, Yemen

### Article History:

**Received:** 16-October-2024,

**Revised:** 2-November-2024,

**Accepted:** 7-December-2024,

**Available online:** 28 February 2025.

## 1. INTRODUCTION

The Precambrian basement rocks of Yemen represent the southern extension of the Arabian Nubian Shield (ANS) and cover an area of approximately 150,000 Km<sup>2</sup> of the total area of the country [1, 2]. These rocks are exposed in the northwestern parts (Sadah-Hajah regions), southwestern parts (Taiz region), and central parts (Al-Bayda region) with small exposures East of Al-Mukalla and small erosional remnants along the Red

Sea Coast (Fig.1). These basement rocks are composed of migmatized gneisses formed under conditions of medium-to high-grade amphibolite facies (e.g. [3–9] with volcanosedimentary belts metamorphosed in the green schist facies in the internal parts, whereas at the edges, they have to varying extents been affected by granitic intrusions [10]. Within the Precambrian outcrops of Yemen, there is evidence of extensive acidic and mafic magmatic activity that ranges from early syntectonic to late tectonic or anorogenic [11–13]. Such mafic magma-

tism has been documented within the Arabian Nubian Shield in the western part of Saudi Arabia (for example, [14–18][14-18], Egypt (for example, [19–22], Yemen (for example, [3, 23] and Sudan (for example, [24, 25]. This mafic magmatism is represented by the older metagabbros, which have been regionally metamorphosed during the Neoproterozoic (~ 850-780) and the younger gabbros, which are mostly fresh and unmetamorphosed during ~ 620-590 Ma in a post-collisional regime following the late stages of arc amalgamation in the Arabian Nubian Shield (refer to the previous references).

The study areas (Al-Maqatirah and Al-Ahkum) are situated on the southwestern outcrops of the basement rocks of Yemen, which are located in the SE of the Taiz governorate (See Fig. 1) and separated from the central block by the Ad Dali graben, which is related to the Najd Fault system [10]. The basement rocks of SE Taiz are considered to be of Precambrian age [26–30], [10] and can be correlated well with recently dated rocks in the central block (Abas and Al-Bayda terranes), which yielded ages up to 2.53 Ga [11, 13] (See Fig.1).

## 2. GEOLOGICAL SETTING

Al-Maqatirah and Al-Ahkum areas are located in the SE Taiz governorate, approximately 76 km and 70 km from Taiz City, respectively, near Al-Turbbah Town. Both areas were covered by various types of rocks ordered in this study according to their relative ages, field relations, and observations. These rocks comprise the basement rocks, followed by a thick sequence of sedimentary rocks, and finally by younger dykes that dissected all of the older rocks (Figs. 2 and 3).

The basement rocks in the Al-Maqatirah and Al-Ahkum areas are represented by gneisses, migmatites, schists, and amphibolites that have undergone medium- to high-grade regional metamorphism during the Pan-African orogeny [13, 29, 31], [4–9]. These rocks were intruded by gabbroic and granitic rocks, mafic/felsic dykes, and veins belonging to this period [32] or younger periods and covered in many parts by sedimentary rocks (Fig. 4a). The gneisses are the dominant rocks that show gray to pinkish gray colors and a strongly foliated structure composed of alternating technocratic and melanocratic bands. They are subjected to a high degree of migmatization and deformation (folding and faulting). Migmatites are widely developed and exhibit various types of structures, such as stromatic (layered), phlebitis (veined), and ophthalmic (augen) migmatites [33]. The schist rocks are exposed in Wadi Al-Ahkum within gneisses and have light gray to gray colors, fine-to-medium-grained texture, and foliated structure. Amphibolites occur as uncomfortable lateral elongated bands intercalated with gneisses, mostly in the NE-SW direction. They are variably altered with gray to greenish-gray colors, foliated structures, and medium-grained textures.

Granitic rocks occur as intrusions, plugs, small dykes, and off-shoots intruding and crossing the basement rocks and gabbroic intrusions (See Figs. 2 and 3), and sometimes contain xenoliths of these rocks. Granitic intrusions are mostly fresh, highly fractured, and pink-to-pinkish grey in color. Their textures vary from coarse-grained central parts to fine-grained and ability textures toward their peripheries. Field relations indicated that the granitic intrusions were younger than the gabbroic intrusions and most likely derived from different sources. The Granitic plugs, dikes, and off-shoots are distributed throughout the study areas in several directions and have variable thicknesses (< 1m to a few meters).

The sedimentary rocks are represented by a thick sequence of the Cretaceous Al-Tawilah Sandstone Group, which occurs as horizontal strata that unconformably overlie the basement rocks in many parts of the study area (See Fig. 4a).

Finally, all these rocks are crossed by numerous dikes of basaltic composition, which represent the youngest rock units in the study areas (mostly of Tertiary age). They have variable thicknesses (up to a few meters) and are mostly oriented in a NW-SE direction parallel to the Red Sea trend. In the following sections we give a detailed field and petrographic descriptions and geochemical study on some gabbroic intrusions from Al-Maqatirah and Al-Ahkum areas, which are the topic of this paper.

## 3. FIELD AND PETROGRAPHY

The gabbroic intrusions from the Al-Maqatirah and Al-Ahkum areas invaded the basement rocks with sharp contacts between them (Fig. 4b) and sometimes contained xenoliths of these rocks (Figs. 4 c & d). These intrusions have irregular shapes but are mostly elongated in the NE-SW direction (See Figs. 2 and 3). They have dark grey, grey, and greenish black colors, coarse-to medium-grained texture (Fig. 4e), and massive structure, but sometimes they show a layered structure (Fig. 4f). They are variably altered, fractured, and dissected by faults and cracks in several directions. They were also crossed by small veinlets filled with secondary minerals (calcite and silica). These gabbroic intrusions were invaded by younger granitic intrusions, dikes, and plugs that sometimes contained xenoliths (Fig. 4g).

Under a microscope, these gabbroic intrusions have a holocrystalline coarse- to medium-grained texture and are composed of plagioclase, pyroxene, hornblende, olivine, and biotite, with apatite, spinel, iron oxides, and sulfides as accessory minerals. Secondary minerals are represented uralite, tremolite-actinolite, serpentine, chlorite, zoisite, epidote, biotite, sericite, calcite, clay minerals, goethite and "limonite." These gabbroic intrusions are unmetamorphosed but variably altered and show some indications of deformation by subsequent events, such as deformed twinning. According to the abundance

and appearance of major mineral constituents, the gabbroic rocks from the Al-Maqatirah and Al-Ahkum areas were classified into the following types:

**Normal gabbro** is composed of plagioclase and pyroxene (augite), with small amounts of hornblende, biotite, apatite, and iron oxides (Fig. 5a). **Olivine gabbro** is composed of olivine, plagioclase, pyroxene, and opaque minerals (Figs. 5b). Olivine crystals are cracked, variably altered to "iddengisite" (reddish brown), serpentine/chlorite (green) and opaque minerals (black) and forming cumulate and intercumulus textures with plagioclase (See Figs. 5b). Most olivine crystals formed kelyphitic structures (Fig. 5c), which were interpreted to be the result of reactions between plagioclase and olivine [34]. **Olivine-pyroxene gabbro** is composed of pyroxene, olivine, plagioclase, and opaque minerals (Fig. 5d). Some pyroxene crystals included completely or partially plagioclase crystals that formed ophitic and subophitic textures, or contained olivine grains that formed poikilitic texture. Some large pyroxene crystals contain small lamellae of orthopyroxene and opaque minerals, forming exsolution textures (Fig. 5e).

**Olivine-biotite gabbro** is composed of plagioclase, olivine, and biotite with small amounts of hornblende, pyroxene, apatite, and opaque minerals (Fig. 5f). Most olivine crystals are mantled by biotite and sometimes hornblende (See Fig. 5f), which can be attributed to complex multivariant reactions involving Fe-Ti oxide minerals, plagioclase, and olivine [35]. These rocks are affected by Na-rich fluid fluxes, as indicated by the presence of rare prismatic crystals of aegirine-augite (highly altered to hornblende) [36], and the formation of a Na-rich zone mantled the Ca-plagioclase crystals.

**Pyroxene gabbro** is composed of pyroxene, plagioclase, and opaque minerals with a small amount of hornblende, biotite, and apatite (Fig. 6a). Pyroxene crystals are variably (Al-Maqatirah intrusion) to completely alter (Al-Ahkum intrusion) to uralite, hornblende, chlorite, clinzoisite, epidote, tremolite-actinolite, and opaque minerals, forming a schiller texture (Fig. 6b). Some altered crystals completely included plagioclase crystals that formed a blastophitic texture. **Hornblende gabbro** is composed of hornblende, plagioclase, pyroxene, and biotite (Fig. 6c), with small amounts of apatite, phlogopite, and opaque minerals. Hornblende crystals show strong pleochroism ( Fig. 6c) and occur as the primary phase of large to medium equant crystals and as the second phase of small crystals associated with biotite, feldspar, quartz, and sometimes apatite. Secondary hornblende was formed after pyroxene. They are fresh and variably altered into uralite, chlorite, tremolite-actinolite, biotite, and opaques.

**Layered gabbro** is exposed in the Al-Ahkum area and is composed of plagioclase, pyroxene, opaques (Fe-Ti oxides), olivine, spinel, and phlogopite. These rocks display lithological alterations of felsic and mafic layers,

forming a rhythmic layering ( Fig. 4f). The felsic layers are dominated by plagioclase (Fig. 6d), whereas the mafic layers are dominated by pyroxene, Fe-Ti oxides, olivine, and spinel and display cumulus and intercumulus textures (Fig. 6e). The cumulus minerals are pyroxene, olivine, and plagioclase where Fe-Ti oxides and spinel are the dominant intercumulus phases. Some pyroxene (Augite) crystals mantled by reaction rims of phlogopite and tremolite-actinolite against opaque minerals and other crystals contain orthopyroxene (enstatite) and opaque minerals (Fig.6f), indicating inversion from pigeonite [37]. Opaque minerals accounted for up to 40% of the mafic layers. Large opaque crystals mostly engulfed and corroded the early formed crystals of pyroxene, plagioclase, and pyroxene, forming reaction rims of phlogopite. Small anhedral green crystals of spinel (hercynite) were enclosed in and associated with opaques.

## 4. GEOCHEMISTRY

The results of representative chemical analyses of the major elements and some trace elements of the gabbroic rocks from the Al-Maqatirah and Al-Ahkum areas are given in table 1.

### 4.1. ANALYTICAL METHODS

42 samples of the gabbroic rocks from the study areas were analyzed for major oxides ( $\text{SiO}_2$ ,  $\text{Al}_2\text{O}_3$ ,  $\text{TiO}_2$ ,  $\text{Fe}_2\text{O}_3$ ,  $\text{MnO}$ ,  $\text{CaO}$ ,  $\text{MgO}$ ,  $\text{K}_2\text{O}$ ,  $\text{Na}_2\text{O}$ ,  $\text{P}_2\text{O}_5$  and  $\text{SO}_3$ ) and trace elements (Cr, Sr, V, and Ba). Twelve of these were analyzed in the Amran Cement Plant, Yemen, using the XRF unit model ARL 9800 XP SIM-SEQ XRF with integrated XRD for major oxides and some trace elements. This XRF device unit was manufactured by Thermo Electron Corporation and used the Rh-tube and UniQuant programs. The UniQuant was fully calibrated and installed in the factory using a universal goniometer. The other 30 samples were analyzed in the Al Barh Cement Plant, Yemen, using an MXF-2100 MULTI-CHANAL Rh-tube X-ray Fluorescence Spectrometer.

Chemical analyses in both XRF devices were performed using pressed powder pellets. The preparation of powder pellets for analyses included sample crushing using JAW CRUSHER, followed by grinding to a fine powder using a Disk Vibration Mill. At this stage of sample preparation, approximately 6-7 ml of hexane ( $\text{C}_6\text{H}_{14}$ ) was added to the crushed sample to decrease the grinding temperature. Subsequently, the fine powder of each sample was placed in a separate circular metallic disk (approximately 5 cm in diameter and 1 cm in height), which was compressed to form a hard disk using a Briquetting Machine Mp-35. The Fe content of the samples analyzed in the Amran Cement Plant is given as  $\text{Fe}_2\text{O}_{3T}$ ,  $\text{FeO}_T$ ,  $\text{FeO}$ , and  $\text{Fe}_2\text{O}_3$  were calculated using the equations  $\text{FeO}_T = \text{Fe}_2\text{O}_{3T} * 0.8998$ ,  $\text{FeO} = \text{FeO}_T * (1 -$

0.15) and  $\text{Fe}_2\text{O}_3 = \text{FeO}_T \cdot 0.15$ , respectively, using the GeoPlot program (A VBA program for geochemical data plotting, Version: 1.0, Build: 060405, programmed by Jibin Zhou). Ti, Cr, V, Sr, and Ba in ppm were derived from  $\text{TiO}_2$ ,  $\text{Cr}_2\text{O}_3$ ,  $\text{V}_2\text{O}_5$ , SrO, and BaO using OXDPPM, a FORTRAN software program to convert chemical elements between oxides and native elements [38].

## 4.2. RESULTS

### 4.2.1. Classification

The gabbroic intrusions from the Al-Maqatirah and Al-Ahkum areas are plotted within or close to the field of gabbro (Fig. 7) using the  $\text{Na}_2\text{O}+\text{K}_2\text{O}$  versus  $\text{SiO}_2$  classification diagram in [39]. In addition, the majority of the studied gabbroic rocks fall in the field of low-Ti ophiolite on the  $\text{TiO}_2$  -  $\text{FeO}_T/\text{FeO}+\text{MgO}$  diagram [40] (Fig. 8a) and in the fields of low-MgO - low  $\text{TiO}_2$  basalts and very low  $\text{TiO}_2$  on the  $\text{TiO}_2$  - MgO diagram [41] (Fig. 8b), but few samples from the Al-Ahkum intrusion trended toward the field of  $\text{TiO}_2$ -rich alkaline basalts. The majority of these samples fall within the field of low-Ti basalts on the  $\text{TiO}_2$ -MgO# diagram [42], but some samples from the Al-Ahkum intrusion straddle between the high-Ti and low-Ti fields (Fig. 8c).

### 4.2.2. Effects of hydrothermal alteration

The effect of alteration on the studied gabbroic rocks is evident from petrography (the formation of secondary minerals) and chemistry (loss on ignition, LOI). Therefore, it is necessary to evaluate the effects of alteration on these rocks. To do this, we drew the analyzed samples on the  $\text{Na}_2\text{O}/\text{K}_2\text{O}$  vs.  $\text{Na}_2\text{O}+\text{K}_2\text{O}$  binary diagram [43] (Fig. 9a) and  $\text{CaO}/\text{Al}_2\text{O}_3$ -MgO/10- $\text{SiO}_2/100$  ternary diagram [44] (Fig. 9b). In these diagrams, the majority of the samples fall in the field of fresh rocks, indicating the small effect of hydrothermal alteration on these rocks.

Furthermore, the low LOI of the analyzed samples (0.001-1.04), except for two samples with high LOI (sample 1.2\*4 = 2.94 and sample 2.2A = 5.37), the lack of obvious correlation between LOI and mobile elements (e.g., K, Ba, Sr, Na) [45], not shown), and the oxidation ratio [ $\text{Fe}_2\text{O}_3/(\text{FeO}+\text{Fe}_2\text{O}_3)$ ] (0.15 to 0.17, See Table 11), illustrates the effect of alteration [46], indicating little effect of alteration on the whole-rock compositions of the studied gabbroic rocks.

### 4.2.3. Fractional crystallization

The majority of the major oxides (wt. %) of the gabbroic rocks from Al-Maqatirah and Al-Ahkum areas show a range of compositions with some samples show anomalous low or high concentrations (denoted by their names after oxide range):  $\text{SiO}_2$  (40.05-51.60; samples M15=53.96 and 1.2X3=54.05),  $\text{TiO}_2$  (0.15-2.94; samples M2.3=4.21, 1.2\*4=6.69 and 2.3A=6.14),  $\text{Al}_2\text{O}_3$  (11.39-32.16; samples 1.2\*4=6.27, M2.5=7.16

and 2.2A=8.96),  $\text{Fe}_2\text{O}_3$  (0.60-3.19; sample M15=0.29), FeO (3.42-18.07; sample M15=1.63), MnO (0.02-0.29), MgO (0.87-8.96; samples M2.5=16.32 and 2.2A=18.81), CaO (6.61-11.79),  $\text{K}_2\text{O}$  (0.17-1.87; sample M2.5=0.07),  $\text{Na}_2\text{O}$  (1.33-5.92; sample M2.5=0.84) and  $\text{P}_2\text{O}_5$  (0.00-4.67). These compositional variations reflect the mineral phases that form these rocks, where the anomalously low or high concentrations of some oxides reflect the relative amount of a specific mineral phase (e.g., the high concentration of  $\text{TiO}_2$  and Fe-oxides refers to a high amount of Fe-Ti oxides; high MgO refers to the presence of olivine).

The correlations between the whole-rock major element oxides are presented in the Harker diagram (Fig. 10). This diagram shows the following trends with increasing  $\text{SiO}_2$  (evaluation of magma): (1) MgO, CaO, and  $\text{Cr}_2\text{O}_3$  were negatively correlated, whereas  $\text{Al}_2\text{O}_3$  showed a weak negative correlation, which could reflect the crystallization of pyroxenes and calcic plagioclase from the early stages; (2)  $\text{TiO}_2$ , FeO,  $\text{Fe}_2\text{O}_3$  and  $\text{V}_2\text{O}_5$  are negatively correlated, which reflects the formation of Fe-Ti oxides; (3)  $\text{Na}_2\text{O}$  is positively correlated, which is related to the formation of Na-feldspar; (4)  $\text{K}_2\text{O}$  did not show a clear trend due to the mobility of this oxide by hydrothermal alteration to which these rocks were subjected. In addition, we noted the absence of compositional gaps between the gabbroic intrusions from the Al-Maqatirah and Al-Ahkum areas (See Fig. 10).

### 4.2.4. Magma type

The studied gabbroic intrusions straddle between the alkaline and sub-alkaline fields on the TAS diagram (See Fig. 7), indicating the transitional character of magma from alkaline to sub-alkaline magma series. The sub-alkaline samples fall in the field of the tholeiitic magma series when plotted on the AFM diagram [47] (Fig. 11).

### 4.2.5. Tectonic setting

Different discrimination diagrams were used to determine the tectonic setting in which the gabbroic intrusions were formed. Based on the Ti/V ratios of the rocks from different tectonic settings (Fig. 12a), these gabbroic rocks fall in lower V and Ti abundances, with Ti/V ratios between 50 and 100, indicating that they have an Ocean Island Basalt (OIB) signature. On the  $\text{Al}_2\text{O}_3$ - $\text{TiO}_2$  diagram [48] (Fig. 12b), the majority of the studied gabbroic rocks fall within the field of arc-related magma setting, with few samples falling within a plat-related magma setting.

## 4.3. DISCUSSION AND PETROGENESIS

The gabbroic intrusions from the Al-Maqatirah and Al-Ahkum areas are plotted within the field of gabbro, except for two samples moving toward the field of diorite (See Fig. 7), which can be attributed to the increase in silica content owing to the subsequent effects of the



hydrothermal solutions (silicification process). However, the evaluation of the effects of hydrothermal alteration indicated little or little effect on these gabbroic rocks (See Figs. 9 a and b). Hence, the analyzed samples were suitable, and the obtained data were representative of their original igneous compositions.

These gabbroic intrusions were classified as low-Ti intrusions ( Figs. 8 a, b, and c). The low-Ti magma is characteristic of an intra-oceanic island arc setting [49] formed in a subduction zone setting [50] by partial melting and re-melting of depleted mantle peridotite [51, 52]. Additionally, low-Ti magma is formed by high-degree partial melting of the peridotite mantle source at shallower depths [53–55]. The few samples from the Al-Ahkum intrusion that straddle the boundary between high-Ti and low-Ti fields or moved toward the High-Ti field can be interpreted by sub-surface mixing of contemporaneous magma batches with low Ti and high Ti compositions [56].

The gabbroic rocks from the Al-Maqatirah and Al-Ahkum areas display a range of major elements that reflect their mineralogical compositions. In addition, the correlation trends between whole-rock major oxide compositions and the absence of compositional gaps between the gabbroic intrusions from the Al-Maqatirah and Al-Ahkum areas (See Fig. 10) lead us to conclude that both intrusions were derived from the same magma source by fractional crystallization processes. In other words, the coherent trends in the variation diagrams of these gabbroic intrusions indicate their derivation from the same magma, and the compositional variations are the result of fractional crystallization processes.

The low MgO (0.87-8.96 wt%), low Mg# (19.95-44.64) and low Cr (96-435 ppm) of all samples, except sample No. 2.2A (MgO = 18.81 wt%, Mg# = 71.82, and Cr = 1258 ppm) and sample No. M2.5 (MgO = 16.32 wt%, Mg# = 58.75 and Cr = 472 ppm), indicated that the studied gabbroic rocks are derived from primary or primitive magma subjected to significant degrees of fractional crystallization. Sample 2.2A can be considered as representative of the composition of the primary magma from which these gabbroic rocks were formed. A similar conclusion was reported by [3], who mentioned that gabbroic rocks within the basement rocks of the Al-Hamurah area, which are located in the NE of the study area, are derived from a mantle source subjected to significant degrees of fractional crystallization.

These gabbroic intrusions display a transitional character from alkaline to sub-alkaline (tholeiitic) magma series (See Figs. 7 and 11) and have an oceanic island basalt (OIB) signature (See Fig. 12a). In addition, the majority of samples fall within the field of arc-related magma setting, with few samples falling within the field of plate-related magma setting (See Fig. 12b). In fact, the OIB that has been used to explain intraplate magmatism on the Earth's surface (e.g., [57, 58] with subalkalic (tholei-

itic) and alkalic compositions [59] can also be formed in an arc-related tectonic setting [60, 61]. The OIB magma, including alkalic and subalkalic (tholeiitic) compositions [59], comprised the derivation of magma by variable partial melting of the mantle source at various depths during the change from arc to intraplate setting [62].

The coexistence of rocks with arc- and ocean island basalt (OIB)-like geochemical signatures in the same magmatic complex has been reported in many localities (e.g [63–68]). Many ideas have been proposed to interpret both signatures to be related to slab roll-back, foundering, tearing, and delamination after collection, [68–70] or to ascending mantle plume (for example, [65]), and to subduction zone (for example, [71, 72] and migration of an extinct ridge, for example, [66]. In addition, the transition from OIB to arc-like compositions can be formed due to contamination by the assimilation of crustal materials [73]. Furthermore, the occurrence of mafic intrusion with an OIB-like signature suggests lithospheric attenuation and significant upwelling of the asthenosphere caused by continental rifting [74] which mostly occurred during the formation of the Arabian lithosphere.

On the other hand, the Arabian–Nubian Shield is formed by accretion and collision of juvenile arc terranes with a high rate of juvenile magmatic addition [75–79] where mantle plume material is thought to play an important role via accretion of the oceanic plateau [80–82]. In addition, trace element enrichment of some plutonic rocks within the Arabian-Nubian shield occurred prior to subduction (i.e., plume material) or after subduction (slab component) [83].

Finally, the studied gabbroic intrusions are unmetamorphosed and can be well compared with similar gabbroic intrusions in the Arabian-Nubian shield from Saudi Arabia [84], which were emplaced post-collision at the end of the Pan-African Orogeny and generated from mafic magma derived from a peridotite mantle source with an arc-like signature related to the previous subduction event in the Arabian–Nubian Shield.

Based on the previous discussion, we conclude that the gabbroic intrusions from the Al-Maqatirah and Al-Ahkum areas are derived from magmas and have OIB character generated in the within-plate and arc-related tectonic setting related to the subduction zone during the formation of the Arabian lithosphere beneath the study area (Arabian-Nubian Shield) and suffered from the interaction of magma with crustal rocks along the route to the surface (crustal contamination).

## 5. SUMMARY AND CONCLUSIONS

The Al-Maqatirah and Al-Ahkum areas are located in the SE of the Taiz governorate within the southwestern outcrops of the basement rocks of Yemen, which represent the southern extension of the Arabian Nubian

Shield (ANS). This paper focuses on the study of gabbroic intrusions that have invaded these basement rocks in these areas. Based on the field work, petrography, and geochemistry, we present the following summary and conclusions.

- The studied gabbroic intrusions have dark grey, grey, black, and greenish black colors, coarse to medium-grained textures, and massive, fractured, and sometimes layered structures. They were invaded by younger granitic intrusions, dikes, plugs, and off-shoots.
- Petrographical studies indicate that these intrusions are unmetamorphosed but sometimes affected by Na-rich fluid fluxes, as evidenced by the presence of rare prismatic crystals of aegirine-augite and the formation of Na-rich zones mantled by Ca-plagioclase crystals. These gabbroic rocks are variably altered and their mineral constituents show many textures and structures. These gabbroic rocks are classified as normal gabbro, olivine gabbro, olivine-pyroxene gabbro, olivine-biotite gabbro, pyroxene gabbro, hornblende gabbro, and layered gabbro.
- Based on geochemistry, the effects of hydrothermal alteration on the geochemical characteristics of these gabbroic intrusions were small, and the obtained data were representative of their original igneous compositions.
- These gabbroic intrusions are classified as low-Ti intrusions generated from the low-Ti magma characteristics of an intra-oceanic island arc setting and formed in a subduction zone setting by partial melting and re-melting of the depleted peridotite mantle source. Some samples from the Al-Ahkum intrusion that strides the boundary between high-Ti and low-Ti fields or moved toward the high-Ti field can be interpreted as sub-surface mixing of contemporaneous magma batches with low-Ti and high-Ti compositions.
- The major element compositions of these gabbroic rocks reflect their derivation from primitive magma subjected to significant degrees of fractional crystallization.
- These gabbroic intrusions have an ocean island basalt (OIB) signature and transitional character of magma from alkaline to sub-alkaline (tholeiitic) magma series, which indicate their derivation by variable degrees of partial melting of the mantle source at various depths during the change from arc to intraplate setting. In addition, the OIB signature of these mafic intrusions suggests lithospheric attenuation and significant upwelling of the asthenosphere caused by continental rifting, which mostly occurs during the formation of the Arabian lithosphere.
- Finally, the studied gabbroic intrusions can be compared with similar gabbroic intrusions in the Arabian-Nubian shield from Saudi Arabia, which are emplaced

post-collision at the end of the Pan-African Orogeny and generated from mafic magma derived from a peridotite mantle source.

## 6. FUTURE RECOMMENDATIONS

We strongly recommend conducting future trace and rare earth element (REE) analyses for better understanding and proper interpretation of the genesis of these gabbroic intrusions and their relationships with the formation of the Arabian-Nubian Shield and ascending Afar mantle plume.

## 7. ACKNOWLEDGMENTS

Praise Allah, the Almighty, for his guidance and support. We extend our sincere gratitude to Prof. Dr. Abdo Sharaf Ghalib for their invaluable guidance. We are deeply thankful to Prof. Dr. Mahyoub Al-Buhairi for his assistance. Finally, we are grateful to the faculty members of the Department of Geology at Taiz University

## REFERENCES

- [1] S. A. AL-KHIRBASH, M. M. SOLIMAN, and A. O. BA-ISSA, "Geochemistry and origin of migmatites of al-zurbi metamorphic belt, sw taiz, republic of yemen," *Earth Sci.* **8** (1995).
- [2] A. Kroner, "Late precambrian plate tectonics and orogeny: a need to redefine the term pan-african," *Afr. geology* (1984).
- [3] M. A. Nasher, "Petrology, geochemistry and mineralization of al-hamurah area, se taiz, republic of yemen," Master's thesis, Cairo University, Egypt (2005).
- [4] A. Malek, "Petrological and geochemical studies on wadi shiban gneisses, taiz, republic of yemen," *Assiut Univ.* (2006).
- [5] A. Malek, "Geological study on hifan area, south east taiz, yemen," *Assiut Univ.* (2010).
- [6] A. A. Ahmed, S. Arai, M. A. A. El-Rus, *et al.*, "Petrology and geochemistry of wadi shiban gneisses taiz, yemen," in *4th International Conference of Geology of Africa, Assiut University*, (2005), pp. 237–265.
- [7] M. A. A. El-Rus, A. Andresen, A.-E. A. Ahmed, and A.-H. Malek, "A clockwise pt path of anatectic metapelites from wadi shiban: implication for crustal evolution in southwestern yemen," (2008).
- [8] A. Malek and A. A. Khudeir, "Deformation history and petrographic inspection on medium to high-grade gneisses and amphibolites, al-kadaha area, sw yemen," *Assiut Univ. J. Geol.* **42**, 1–16 (2013).
- [9] A.-H. Malek and G. M. Al-Ramisy, "Lithology, structural features and geological history of the area in and west of al-turbah town, southwestern yemen," *TURJ* **28** (2022).
- [10] R. G. plc., "Satellite mapping programme: Technical report for yemen joint project for natural resources," *Tech. rep.*, Ministry of Oil and Mineral Resources, Sana'a (1992).
- [11] B. F. Windley, M. J. Whitehouse, and M. A. Ba-Bttat, "Early precambrian gneiss terranes and pan-african island arcs in yemen: crustal accretion of the eastern arabian shield," *Geology* **24**, 131–134 (1996).
- [12] Z. R. Beydoun, M. A. As-Sururi, H. El-Nakhal, *et al.*, *International lexicon of stratigraphy, volume 2nd edition, Republic of Yemen, IUGS publication No. 34* (1998).
- [13] M. J. Whitehouse, B. F. Windley, M. A. Ba-Bttat, *et al.*, "Crustal evolution and terrane correlation in the eastern arabian shield, yemen: geochronological constraints," *J. Geol. Soc.* **155**, 281–295 (1998).
- [14] H. M. Helmy, Y. M. Abd El-Rahman, M. Yoshikawa, *et al.*, "Petrology and sm–nd dating of the genina gharbia alaskan-type



- complex (egypt): insights into deep levels of neoproterozoic island arcs," *Lithos* **198**, 263–280 (2014).
- [15] H. M. Helmy, M. Yoshikawa, T. Shibata, *et al.*, "Sm–Nd and Rb–Sr isotope geochemistry and petrology of Abu Hamamid intrusion, eastern desert, Egypt: an Alaskan-type complex in a backarc setting," *Precambrian Res.* **258**, 234–246 (2015).
- [16] A. A. Surour, A. H. Ahmed, and H. M. Harbi, "Mineral chemistry as a tool for understanding the petrogenesis of Cryogenian (arc-related)–Ediacaran (post-collisional) gabbros in the western Arabian shield of Saudi Arabia," *Int. J. Earth Sci.* **106**, 1597–1617 (2017).
- [17] S. E. Abdallah, S. Ali, and M. A. Obeid, "Geochemistry of an Alaskan-type mafic-ultramafic complex in eastern desert, Egypt: New insights and constraints on the Neoproterozoic island arc magmatism," *Geosci. Front.* **10**, 941–955 (2019).
- [18] S. Ali and A. S. Alshammari, "Genesis of gabbroic intrusions in the Arabian shield, Saudi Arabia: mineralogical, geochemical and tectonic fingerprints of the Neoproterozoic arc magmatism," *Geol. Mag.* **158**, 1639–1656 (2021).
- [19] M. F. El-Ramly and M. Hermina, *Geologic map of the Qena Quadrangle, Egypt* (Egyptian Geological Survey and Mining Authority, 1978).
- [20] M. F. E. Ramly and M. H. Hermina, "Geologic map of the Aswan quadrangle, Egypt, scale 1:500,000," Tech. rep., U.S. Geological Survey, in cooperation with the U.S. Agency for International Development (USAID) (1978).
- [21] M. Takla, F. Basta, M. Madbouly, and A. Hussein, "The mafic-ultramafic intrusions of Sinai, Egypt," *Ann. Geol. Surv. Egypt* **24**, 1–40 (2001).
- [22] M. S. Basta, "Petrology and geochemical characteristic of the younger gabbros of Wadi Shianite area, southeastern desert, Egypt," *Open J. Geol.* **5**, 577–588 (2015).
- [23] M. A. Wahed, B. Zoheir, Z. Hamimi, and K. Al-Selwi, "Tectonic evolution of the Archaean–Neoproterozoic basement complex of Dhi Na'im-al Bayda district, Republic of Yemen," in *Proceedings, 1st International Conference on Geology of the Arab World, Cairo University, Egypt*, (2006).
- [24] T. M. Tawfik, "Geology of Dirbat well area, Red Sea hills, Sudan," Master's thesis, Faculty of Science, Cairo University (1981). Unpublished M.Sc. Thesis, pp. 1–40.
- [25] E. K. El-Sawy, A. EldougDoug, and M. Gobashy, "Geological and geophysical investigations to delineate the subsurface extension and the geological setting of Al Jilani layered intrusion and its mineralization potentiality, Ad Dawadimi district, Kingdom of Saudi Arabia," in *Saudi Society for Geosciences*, (2017), pp. 1–25.
- [26] A. D. Hutchinson, "A review of mineral potential of Yemen Arab Republic," Tech. rep., Prospection Limited, Canada (1970).
- [27] STROJEXPORT, "Project of geological prospection of the Taiz Precambrian and adjacent areas," Tech. rep., YOMINCO/STROJEXPORT, Taiz, Yemen Arab Republic (1970). Unpublished report, 30 p.
- [28] GEOMIN, "Preliminary report on the geological, geophysical and geochemical investigations carried out in Al-Hamurah area," Tech. rep., GEOMIN/YOMINCO (1979). Unpublished report, 66 p.
- [29] GEOMIN, "Report on the geological, mineralogical and geophysical works carried for molybdenite, zircon and radioactive substance in Al-Hamurah area, Yemen Arab Republic," Tech. rep., GEOMIN/YOMINCO, Bucharest (1984).
- [30] J. Michel, J. Corbs, J. Liscuyer, and B. Odent, "Yemen Arab Republic mineral master plan," *Bur Rech Geol Min (BRGM) Rep.* **88**, 1–546 (1989).
- [31] GEOMIN, "Geological report on the mining and drilling works carried out in Al-Hamurah area, Yemen Arab Republic," Tech. rep., GEOMIN/YOMINCO, Bucharest (1984). Unpublished report, 229 p.
- [32] A. S. Ghaleb, "Precambrian mafic rocks of southwestern part of Yemen. Tectonism, magmatism and metalogeny," in *5th International Conference on the Geology of the Middle East*, (2003), pp. 277–286.
- [33] K. Mehnert, *Migmatites and the Origin of Granitic rocks* (Elsevier, Amsterdam, 1968).
- [34] D. T. Claeson, "Coronas, reaction rims, symplectites and emplacement depth of the Rymmen gabbro, Transscandinavian igneous belt, southern Sweden," *Mineral. Mag.* **62**, 743–757 (1998).
- [35] P. R. Whitney and J. M. McLelland, "Origin of biotite-hornblende coronas between oxides and plagioclase in Olivine metagabbros, Adirondack region, New York," *Contributions to Mineral. Petrol.* **82**, 34–41 (1983).
- [36] N. C. Ghose, A. K. Singh, A. Dutt, and S. Imtisonup, "Significance of aegirine-bearing metabasic rocks in the metamorphic evolution of the Nagaland accretionary prism, northeast India," *Geol. J.* **57**, 5207–5221 (2022).
- [37] K. Quadling and R. G. Cawthorn, "The layered gabbro-norite sequence, main zone, eastern Bushveld complex," *South Afr. J. Geol.* **97**, 442–454 (1994).
- [38] A. T. Al-Mishwat, "Oxdppm; a FORTRAN software programme to convert chemical elements between oxides and native elements," *J. Softw. Eng. Appl.* **9**, 561–576 (2016).
- [39] K. G. Cox, J. D. Bell, and R. J. Pankhurst, *The interpretation of igneous rocks* (George, Allen and Unwin, London, 1979).
- [40] G. Serri, "The petrochemistry of ophiolite gabbroic complexes. A key for the classification of ophiolites into low-Ti and high-Ti types," *Earth Planet* **52**, 203–212 (1981).
- [41] R. Laurent and R. Heberer, "The volcanic and intrusive rocks of the Quebec Appalachian ophiolites (Canada) and their island arc setting," *Chem. Geol.* **77**, 287–302 (1989).
- [42] J. M. Millett, M. J. Hole, D. W. Jolley, and S. R. Passey, "Geochemical stratigraphy and correlation within large igneous provinces: The final preserved stages of the Faroe Islands basalt group," *Lithos* **286–287**, 1–15 (2017).
- [43] A. Miyashiro, "Volcanic rock series and tectonic setting," *Annu. Rev. Earth Planet. Sci.* **3**, 251–269 (1975).
- [44] A. Davis, W. H. Bleckburn, W. R. Brown, and W. D. Ehmann, "Trace elements geochemistry and origin of late Precambrian–early Cambrian catocin greenstones of the central Appalachian mountains," Tech. rep., University of California at Davies (1978). Unpublished report.
- [45] J. X. Guan, "Petrogenesis of the Panzhihua-type gabbroic layered intrusions and associated Fe-Ti-V oxide deposits: Insights from mineral chemistry and numerical modeling," Ph.D. thesis, University of Tasmania (2014).
- [46] S. D. Iyer and D. Ray, "Structure, tectonic and petrology of mid-oceanic ridges and the Indian scenario," *Curr. Sci.* **85**, 277–289 (2003).
- [47] T. N. Irvine and W. R. A. Baragar, "A guide to the chemical classification of the common rocks," *Can. J. Earth Sci.* **8**, 523–548 (1971).
- [48] D. Muller and D. Groves, *Potassic igneous rocks and associated gold-copper mineralization*, vol. 56 of *Lecture Notes in Earth Science* (1997).
- [49] L. Beccaluva, G. Macciotta, G. B. Piccardo, and O. Zeda, "Clinopyroxene composition of ophiolite basalts as petrogenetic indicator," *Chem. Geol.* **77**, 165–182 (1989).
- [50] M. Camuzcuoğlu, U. Bağcı, J. Koepke, and P. E. Wolff, "Tectonic significance of the cumulate gabbros within Kuluncak ophiolitic suite (Malatya, SE Turkey) inferred from geochemical data," *Ophiolite* **42**, 81–103 (2017).
- [51] R. Laurent and R. Hébert, "The volcanic and intrusive rocks of the Quebec Appalachian ophiolites (Canada) and their island arc setting," *Chem. Geol.* **77**, 287–302 (1989).
- [52] T. E. Waight and J. A. Baker, "Depleted basaltic lavas from the proto-Iceland plume, central east Greenland," *J. Petrol.* **53**, 1569–1596 (2012).
- [53] Y. Xu, S.-L. Chung, B.-M. Jahn, and G. Wu, "Petrologic and geochemical constraints on the petrogenesis of Permian–Triassic Emeishan flood basalts in southwestern China," *Lithos* **58**, 145–168 (2001).
- [54] X. C. Wang, X. H. Li, W. X. Li, and Z. X. Li, "Ca. 825 Ma komatiitic basalts in South China: First evidence for >1500 °C mantle melts by a Rodinian mantle plume," *Geology* **35**, 1103–1106 (2007).

- [55] L. Zhang, Z.-Y. Ren, M. R. Handler, *et al.*, "The origins of high-ti and low-ti magmas in large igneous provinces, insights from melt inclusion trace elements and sr-pb isotopes in the emeishan large igneous province," *Lithos* **344–345**, 122–133 (2019).
- [56] J. M. Millett, "Geochemical stratigraphy and correlation within the faroe island basalt group with the development in the analysis of large igneous province deposits from well data," Ph.D. thesis, University of Aberdeen (2014).
- [57] J. T. Wilson, "A possible origin of the hawaiian islands," *Can. J. Phys.* **41**, 863–870 (1963).
- [58] M. Wilson, *Igneous Petrogenesis – A Global Tectonic Approach* (London Unwin Hyman, 1989).
- [59] D. Suetsugu, B. Steinberger, and T. Kogiso, "Mantle plumes and hotspots," in *Reference Module in Earth Systems and Environmental Sciences*, (2013).
- [60] B. F. Windley and W. Xiao, "Ridge subduction and slab windows in the central asian orogenic belt: Tectonic implications for the evolution of an accretionary orogen," *Gondwana Res.* **61**, 73–87 (2018).
- [61] F. F. P. Corrales, I. A. Dussin, M. Heilbron, *et al.*, "Coeval high ba-sr arc-related and oib neoproterozoic rocks linking pre-collisional magmatism of the ribeira and araquai orogenic belts, se-brazil," *Precambrian Res.* **337**, 105476 (2020).
- [62] A. M. Abdel-Karim, A. A. El-Awady, H. M. Helmy, *et al.*, "Younger gabbros from egypt: A transition from tholeiitic to alkaline basaltic magma and from arc to within plate rifting regime," in *The 6th Environmental Conference*, (Faculty of Science, Zagazig University, Zagazig, Egypt, 2011), p. 194–220.
- [63] C. Coulon, M. H. Megartsi, S. Fourcade, *et al.*, "Postcollisional transition from calc-alkaline to alkaline volcanism during the neogene in oranie (algeria): magmatic expression of a slab breakoff," *Lithos* **62**, 87–110 (2002).
- [64] X. C. Wang, X. H. Li, W. X. Li, *et al.*, "The bikou basalts in the northwestern yangtze block, south china: remnants of 820–810 ma continental flood basalts?" *Geol. Soc. Am. Bull.* **120**, 1478–1492 (2008).
- [65] K. Wu, M. X. Ling, W. Sun, *et al.*, "Major transition of continental basalts in the early cretaceous: implications for the destruction of the north china craton," *Chem. Geol.* **470**, 93–106 (2017).
- [66] F. Zhang, W. Li, N. C. White, *et al.*, "Geochemical and isotopic study of metasomatic apatite: Implication for gold mineralization in xindigou, north china," *Ore Geol. Rev.* **127**, 103853 (2020).
- [67] F. Nouri, H. Azizi, Y. Asahara, and R. J. Stern, "A new perspective on cenozoic calc-alkaline and shoshonitic volcanic rocks, eastern saveh (central iran)," *Int. Geol. Rev.* **63**, 476–503 (2021).
- [68] Q. H. Yan, H. Wang, Y. Wu, and G. Chi, "Simultaneous development of arc-like and oib-like mafic dikes in eastern guangdong, se china: implications for late jurassic–early cretaceous tectonic setting and deep geodynamic processes of south china," *Lithos* **388–389**, 106021 (2021).
- [69] F. Rabayrol, C. J. Hart, and D. J. Thorkelson, "Temporal, spatial and geochemical evolution of late cenozoic post-subduction magmatism in central and eastern anatolia, turkey," *Lithos* **336–337**, 67–96 (2019).
- [70] B. L. Weaver, "The origin of ocean island basalt end-member compositions: trace element and isotopic constraints," *Earth Planet. Sci. Lett.* **104**, 381–397 (1991).
- [71] Z. Xu, Y.-F. Zheng, and Z.-F. Zhao, "Barium isotope fractionation during dehydration melting of the subducting oceanic crust: Geochemical evidence from oib-like continental basalts," *Chem. Geol.* **594**, 120751 (2022).
- [72] A. Kocaarslan and E. Y. Ersoy, "Petrologic evolution of miocene-pliocene mafic volcanism in the kangal and gürün basins (sivas-malatya), central east anatolia: evidence for miocene anorogenic magmas contaminated by continental crust," *Lithos* **310–311**, 392–408 (2018).
- [73] A. Kocaarslan and E. Y. Ersoy, "Petrologic evolution of miocene-pliocene mafic volcanism in the kangal and gürün basins (sivas-malatya), central east anatolia: evidence for miocene anorogenic magmas contaminated by continental crust," *Lithos* **310–311**, 392–408 (2018).
- [74] G. Feng, Y. Dilek, X. Niu, *et al.*, "Geochemistry and geochronology of oib-type, early jurassic magmatism in the zhangguangcai range, ne china, as a result of continental back-arc extension," *Geol. Mag.* **158** (2018).
- [75] H. J. Duyverman, N. B. W. Harris, and C. J. Hawkesworth, "Crustal accretion in the pan african: Nd and sr isotope evidence from the arabian shield," *Earth Planet. Sci. Lett.* **59**, 315–326 (1982).
- [76] P. R. Johnson and B. Woldehaimanot, "Development of the arabian-nubian shield: perspectives on accretion and deformation in the northern east african orogen and the assembly of gondwana," in *Geological Society, London, Special Publications*, M. Yoshida, B. F. Windley, and S. Dasgupta, eds. (2003), p. 289–325.
- [77] P. J. Patchett and C. G. Chase, "Role of transform continental margins in major crustal growth episodes," *Geology* **30**, 39–42 (2002).
- [78] A. Reymier and G. Schubert, "Phanerozoic addition rates to the continental crust and crustal growth," *Tectonics* **3**, 63–77 (1984).
- [79] R. J. Stern, "Arc assembly and continental collision in the neoproterozoic east african orogen: Implication of consolidation of gondwanaland," *Annu. Rev. Earth Planet. Sci.* **22**, 315–319 (1994).
- [80] M. Stein, "Tracing the plume material in the arabian-nubian shield," *Precambrian Res.* **123**, 223–234 (2003).
- [81] M. Stein and S. L. Goldstein, "From plume head to continental lithosphere in the arabian–nubian shield," *Nature* **382**, 773–778 (1996).
- [82] M. Teklay, A. Kroner, and K. Mezger, "Enrichment from plume interaction in the generation of neoproterozoic arc rocks in northern eritrea: Implications for crustal accretion in the southern arabian-nubian shield," *Chem. Geol.* **184**, 167–184 (2002).
- [83] F. G. Yeshanew, *Crustal evolution of the Arabian–Nubian Shield. Insights from zircon geochronology and Nd–Hf–O isotopes* (Stockholm University, Sweden, 2017).
- [84] S. Ali and A. S. Alshammari, "Genesis of gabbroic intrusions in the arabian shield, saudi arabia: mineralogical, geochemical and tectonic fingerprints of the neoproterozoic arc magmatism," *Geol. Mag.* **158**, 1639–1656 (2021).
- [85] A. Miyashiro, "Nature of alkaline volcanic rock series," *Contributions to Mineral. Petrol.* **66**, 91–104 (1978).
- [86] J. W. Shervais, "Ti-v plots and petrogenesis of modern and ophiolitic lavas," *Earth Planet. Sci. Lett.* **59**, 108–118 (1982).

## 8. LIST OF TABLES AND FIGURES

**Table 1.** Chemical analysis of gabbroic intrusions from Al-Maqatirah area and Al- Ahkum areas.

	Al-Maqatirah area											Al-Ahkum area				
	M18	M15	M2.20	M2.3	M2.5	M2.18	M2.20	M1.20	M1.12	M1.22	M1.22	1.2X4	26	1.2X3	1.3	2.3A
SiO <sub>2</sub>	50.70	53.96	50.17	41.55	44.81	46.70	44.89	43.24	43.34	51.38		48.69	49.64	54.05	51.60	40.05
TiO <sub>2</sub>	1.23	0.45	1.25	4.21	1.91	0.66	0.55	1.32	1.27	0.15		1.99	1.64	1.50	0.68	6.14
Al <sub>2</sub> O <sub>3</sub>	24.13	26.24	24.76	16.56	7.16	25.03	33.81	25.04	25.62	15.01		18.56	23.73	19.84	25.47	11.39
Fe <sub>2</sub> O <sub>3</sub>	0.66	0.29	0.67	1.60	2.02	1.76	1.43	1.60	1.58	1.73		1.51	1.07	0.99	0.60	3.19
FeO	3.75	1.63	3.77	9.04	11.46	8.81	7.15	8.00	7.89	8.64		8.53	6.07	5.63	3.42	18.07
MnO	0.04	0.02	0.03	0.09	0.16	0.17	0.12	0.14	0.14	0.17		0.10	0.08	0.07	0.04	0.22
MgO	1.99	0.87	2.12	6.34	16.32	5.23	1.78	3.44	3.34	5.79		6.88	3.56	3.63	2.76	8.96
CaO	9.21	7.92	9.08	11.65	11.79	6.99	7.36	9.22	9.22	10.73		7.95	8.12	6.66	8.33	7.86
K <sub>2</sub> O	0.56	0.81	0.65	0.17	0.07	1.87	0.53	1.22	1.10	0.32		0.62	0.46	1.14	0.65	0.27
Na <sub>2</sub> O	5.33	5.92	5.08	3.29	0.84	2.38	1.33	2.12	2.19	1.42		3.74	4.51	4.82	4.81	2.25
P <sub>2</sub> O <sub>5</sub>	1.83	0.79	1.59	4.67	2.42	0.07	0.12	4.33	4.07	4.42		0.07	0.19	0.83	0.44	0.55
SO <sub>3</sub>	0.06	0.03	0.09	0.05	0.09	0.21	0.19	0.20	0.20	0.23		0.18	0.10	0.05	0.03	0.22
Cl	0.01	0.01	0.01	0.03	0.02	0.00	0.03	0.00	0.01	0.02		0.03	0.02	0.04	0.01	0.01
Cr <sub>2</sub> O <sub>3</sub>	0.04	0.03	0.01	0.02	0.07	0.00	0.00	0.00	0.00	0.00		0.03	0.04	0.03	0.03	0.03
V <sub>2</sub> O <sub>5</sub>	0.01	0.04	0.01	0.04	0.04	0.00	0.00	0.00	0.00	0.00		0.05	0.03	0.03	0.01	0.14
SrO	0.14	0.14	0.13	0.09	0.02	0.00	0.00	0.00	0.00	0.00		0.07	0.09	0.07	0.10	0.03
BaO	0.07	0.05	0.08	0.03	0.07	0.00	0.00	0.00	0.00	0.00		0.03	0.03	0.07	0.07	0.03
LOI	0.23	0.81	0.50	0.59	0.73	0.11	0.69	0.14	0.03	0.00		0.98	0.62	0.56	0.95	0.61
Total	100.00	100.00	100.00	100.00	100.00	100.00	100.00	100.00	100.00	100.00		100.00	100.00	100.00	100.00	100.00
K <sub>2</sub> O+Na <sub>2</sub> O	5.89	6.73	5.73	3.46	0.92	4.25	1.87	3.34	3.29	1.74		4.36	4.97	5.96	5.45	2.52
Fe <sub>2</sub> O <sub>3</sub> /(FeO+Fe <sub>2</sub> O <sub>3</sub> )	0.15	0.15	0.15	0.15	0.15	0.17	0.17	0.17	0.17	0.17		0.15	0.15	0.15	0.15	0.15
FeO <sub>i</sub> /(FeO <sub>i</sub> +MgO)	0.69	0.69	0.68	0.63	0.45	0.67	0.83	0.74	0.74	0.64		0.59	0.67	0.65	0.59	0.70
Mg#	34.66	34.81	35.97	41.24	58.75	37.24	19.95	30.11	29.73	40.13		44.64	36.97	39.19	44.64	33.15
Ti	7348	2702	7471	25233	11440	3938	3316	7892	7594	888		11905	9812	9010	4054	36829
Cr	248	192	96	138	472	0	0	0	0	0		231	250	181	235	180
V	79	208	79	198	210	0	0	0	0	0		252	188	159	68	765
Sr	1190	1186	1105	727	163	0	0	0	0	0		554	739	601	854	258
Ba	639	413	675	245	600	0	0	0	0	0		257	273	582	606	263

\* Data recalculated to 100 wt. % Mg# = MgO/(MgO+FeO)\*100 FeO<sub>i</sub> = FeO+Fe<sub>2</sub>O<sub>3</sub>

Table 2. Continued

	Al-Ahkum area																
	2.2A	1.2A	2.3A	2C	2.5	2.6	2.7	2.8	1.2*1	1.2*2	1.2*4	1.2A	1.4A	1.2B	1.2D	1.3	
SiO <sub>2</sub>	44.01	46.12	48.04	48.02	45.66	45.92	45.14	46.55	44.83	47.15	46.21	47.17	47.43	49.45	47.43	46.07	
TiO <sub>2</sub>	1.62	2.94	1.56	0.98	0.37	2.00	1.03	0.77	1.14	0.55	6.69	2.65	0.86	0.67	0.62	0.29	
Al <sub>2</sub> O <sub>3</sub>	8.96	21.21	19.63	20.38	32.16	22.05	29.26	25.63	25.38	22.89	6.27	21.43	19.18	20.04	27.17	29.88	
Fe <sub>2</sub> O <sub>3</sub>	1.30	1.62	2.04	1.95	1.39	2.10	1.62	1.75	1.79	2.02	3.05	1.98	1.90	1.84	1.57	1.53	
FeO	7.38	9.17	10.20	9.74	6.97	10.51	8.10	8.75	8.94	10.09	15.25	9.91	9.52	9.18	7.87	7.64	
MnO	0.12	0.10	0.20	0.21	0.13	0.19	0.15	0.16	0.18	0.22	0.29	0.20	0.20	0.20	0.15	0.15	
MgO	18.81	3.24	5.65	6.44	2.42	5.45	2.85	3.87	4.14	6.76	6.48	4.30	5.94	6.51	3.80	3.73	
CaO	9.68	8.95	8.62	7.75	7.65	7.69	7.61	9.16	8.31	6.61	10.38	8.54	9.49	8.37	8.23	7.44	
K <sub>2</sub> O	0.68	0.38	1.06	1.00	0.77	0.90	1.00	0.70	0.77	0.64	0.42	0.74	0.47	0.74	0.58	0.88	
Na <sub>2</sub> O	1.33	4.43	2.47	2.32	1.81	2.15	2.50	1.79	1.99	1.80	1.37	2.05	1.47	1.86	1.71	2.06	
P <sub>2</sub> O <sub>5</sub>	0.37	1.24	0.00	0.56	0.00	0.00	0.34	0.00	1.76	0.00	0.39	0.06	2.75	0.20	0.14	0.04	
SO <sub>3</sub>	0.10	0.07	0.23	0.22	0.21	0.22	0.19	0.20	0.21	0.21	0.24	0.21	0.21	0.21	0.20	0.19	
Cl	0.01	0.05	0.00	0.00	0.02	0.01	0.00	0.00	0.03	0.03	0.02	0.00	0.00	0.01	0.01	0.01	
Cr <sub>2</sub> O <sub>3</sub>	0.18	0.06	0.00	0.00	0.00	0.00	0.00	0.00	0.00	0.00	0.00	0.00	0.00	0.00	0.00	0.00	
V <sub>2</sub> O <sub>5</sub>	0.03	0.06	0.00	0.00	0.00	0.00	0.00	0.00	0.00	0.00	0.00	0.00	0.00	0.00	0.00	0.00	
SiO	0.05	0.08	0.00	0.00	0.00	0.00	0.00	0.00	0.00	0.00	0.00	0.00	0.00	0.00	0.00	0.00	
BaO	0.03	0.06	0.00	0.00	0.00	0.00	0.00	0.00	0.00	0.00	0.00	0.00	0.00	0.00	0.00	0.00	
LOI	5.32	0.21	0.32	0.43	0.44	0.82	0.22	0.68	0.52	1.04	2.94	0.77	0.57	0.73	0.51	0.08	
Total	100.00	100.00	100.00	100.00	100.00	100.00	100.00	100.00	100.00	100.00	100.00	100.00	100.00	100.00	100.00	100.00	
K <sub>2</sub> O+Na <sub>2</sub> O	2.01	4.81	3.53	3.32	2.57	3.04	3.49	2.49	2.76	2.44	1.79	2.80	1.94	2.60	2.28	2.94	
Fe <sub>2</sub> O <sub>3</sub> /(FeO+Fe <sub>2</sub> O <sub>3</sub> )	0.15	0.15	0.17	0.17	0.17	0.17	0.17	0.17	0.17	0.17	0.17	0.17	0.17	0.17	0.17	0.17	
FeO <sub>f</sub> /(FeO <sub>f</sub> +MgO)	0.32	0.77	0.68	0.64	0.78	0.70	0.77	0.73	0.72	0.64	0.74	0.73	0.66	0.63	0.71	0.71	
Mg#	71.82	26.12	35.65	39.80	25.78	34.16	26.03	30.66	31.63	40.10	29.84	30.27	38.40	41.49	32.54	32.81	
Ti	9732	17646	9343	5876	2197	11964	6149	4643	6859	3271	40079	15871	5151	4041	3697	1762	
Cr	1258	435	0	0	0	0	0	0	0	0	0	0	0	0	0	0	
V	177	345	0	0	0	0	0	0	0	0	0	0	0	0	0	0	
Sr	449	651	0	0	0	0	0	0	0	0	0	0	0	0	0	0	
Ba	274	560	0	0	0	0	0	0	0	0	0	0	0	0	0	0	

\* Data recalculated to 100 wt. %

Mg# = MgO/(MgO+FeO)\*100

FeO<sub>f</sub> = FeO+Fe<sub>2</sub>O<sub>3</sub>

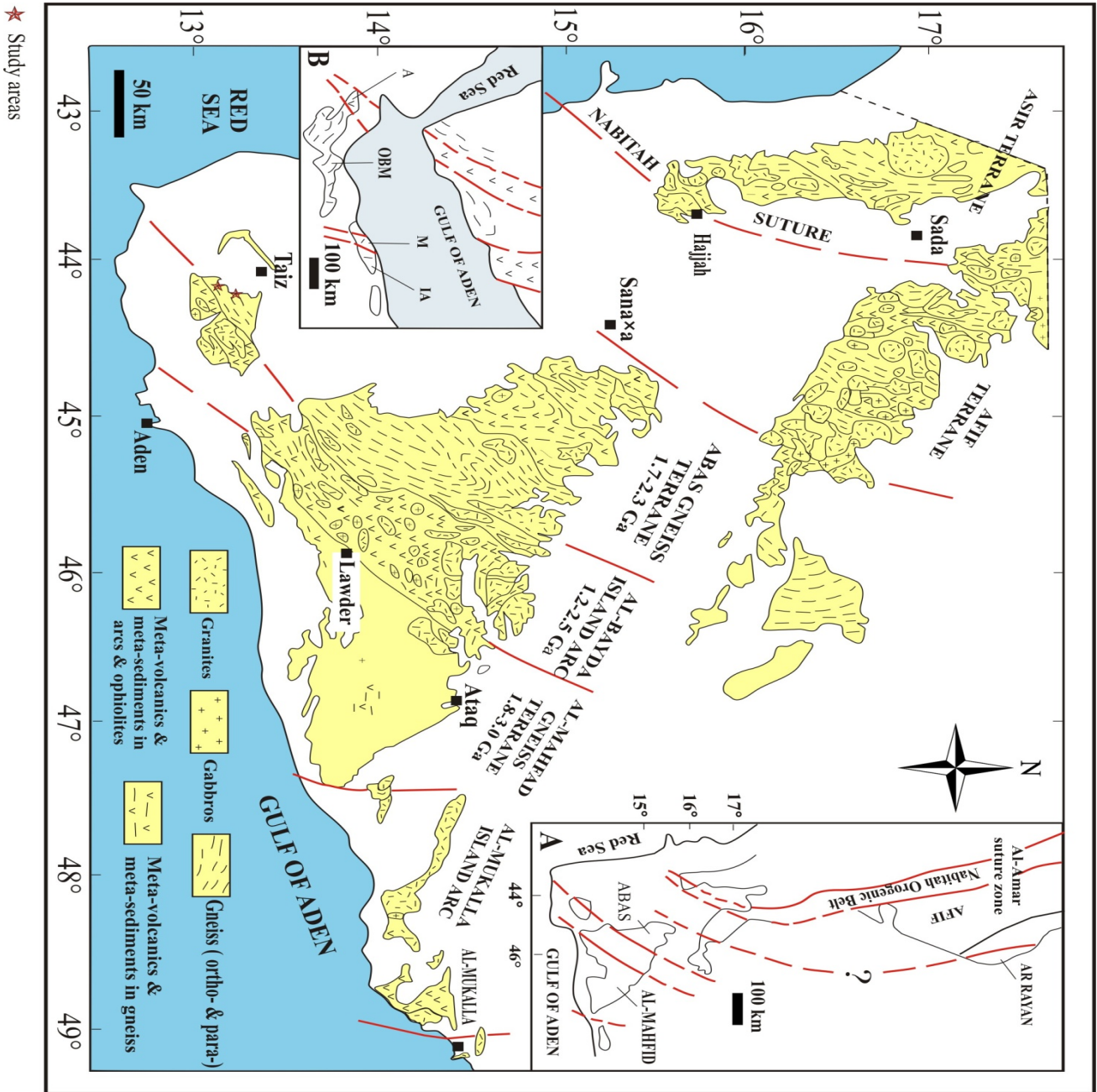


**Figure 1.** Precambrian outcrops map in Yemen showing delineation of gneisses and island arcs terranes and correlations with adjoining areas in Saudi Arabia (A) and northern Somalia (B) (after [11]).

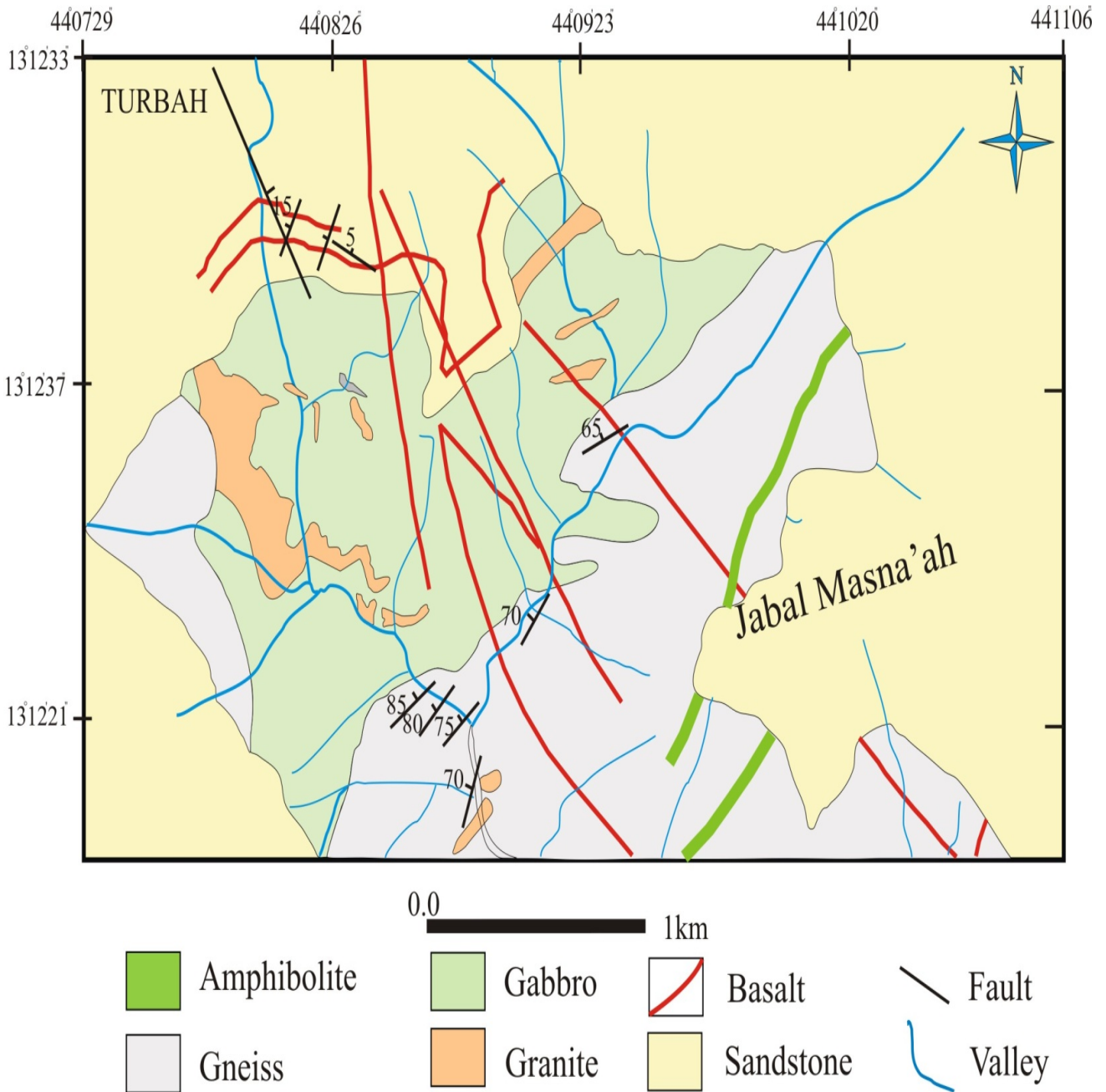


Figure 2. Geological Map of Al-Maqatirah area (Modified After [29]).

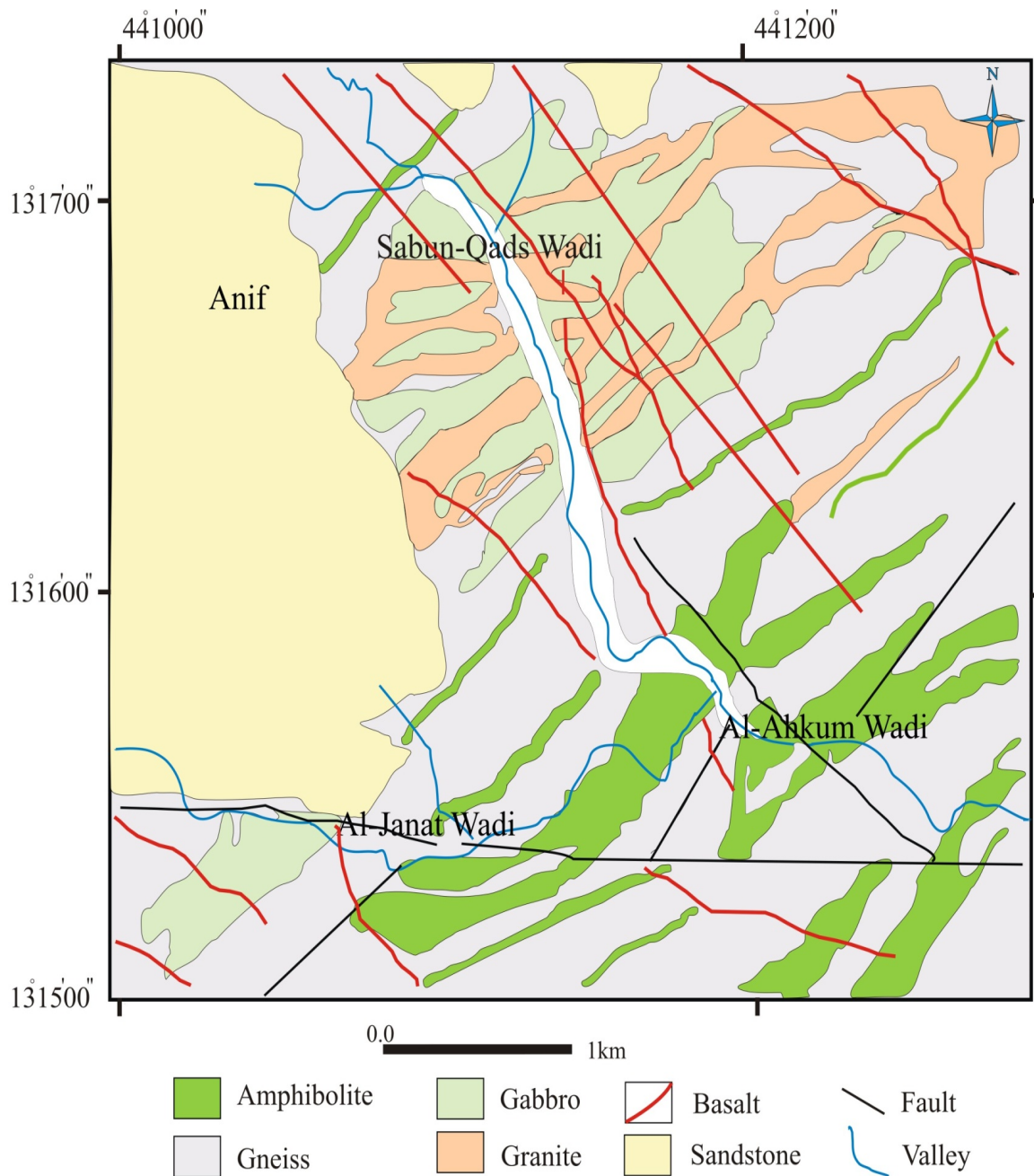
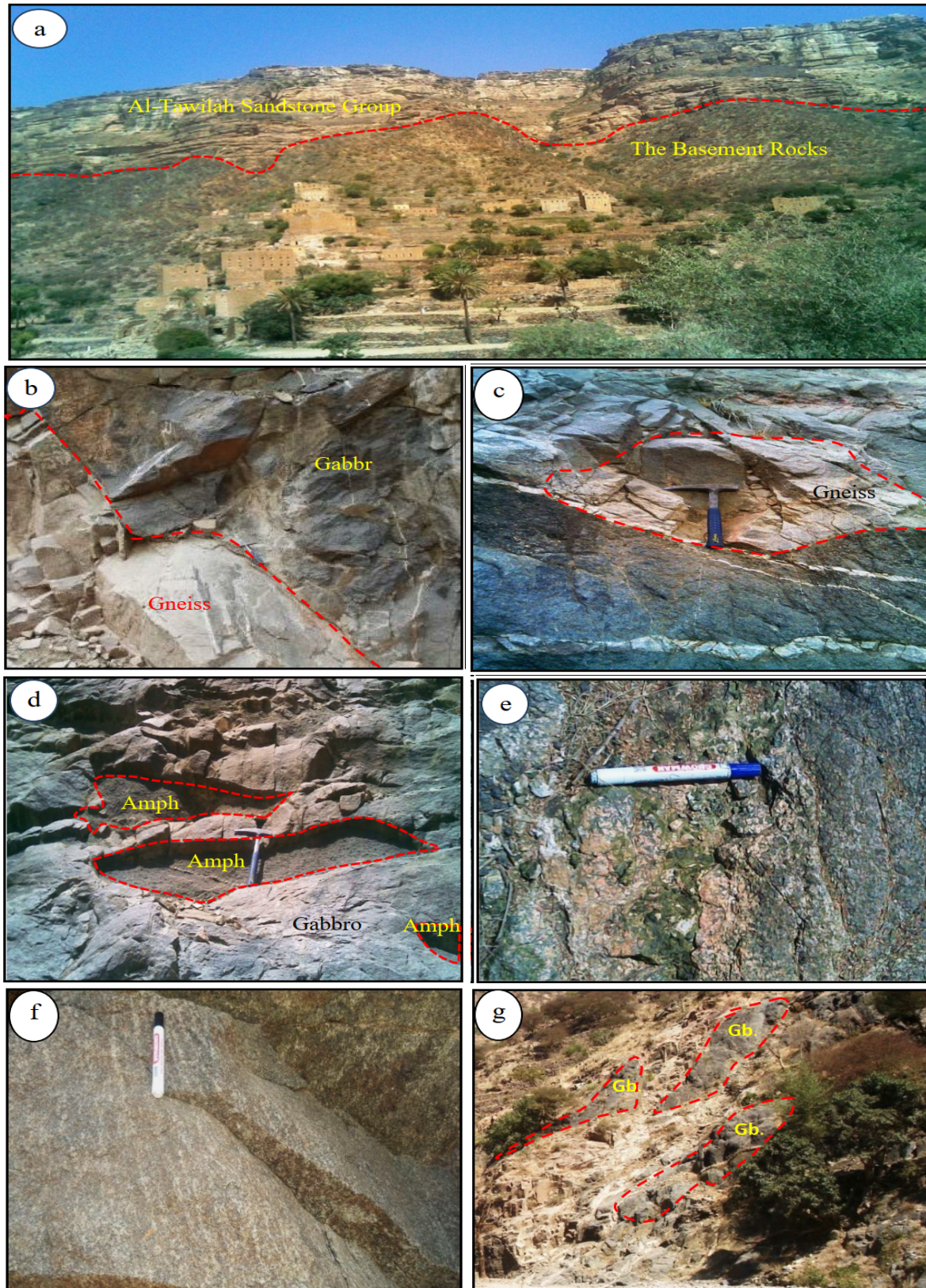
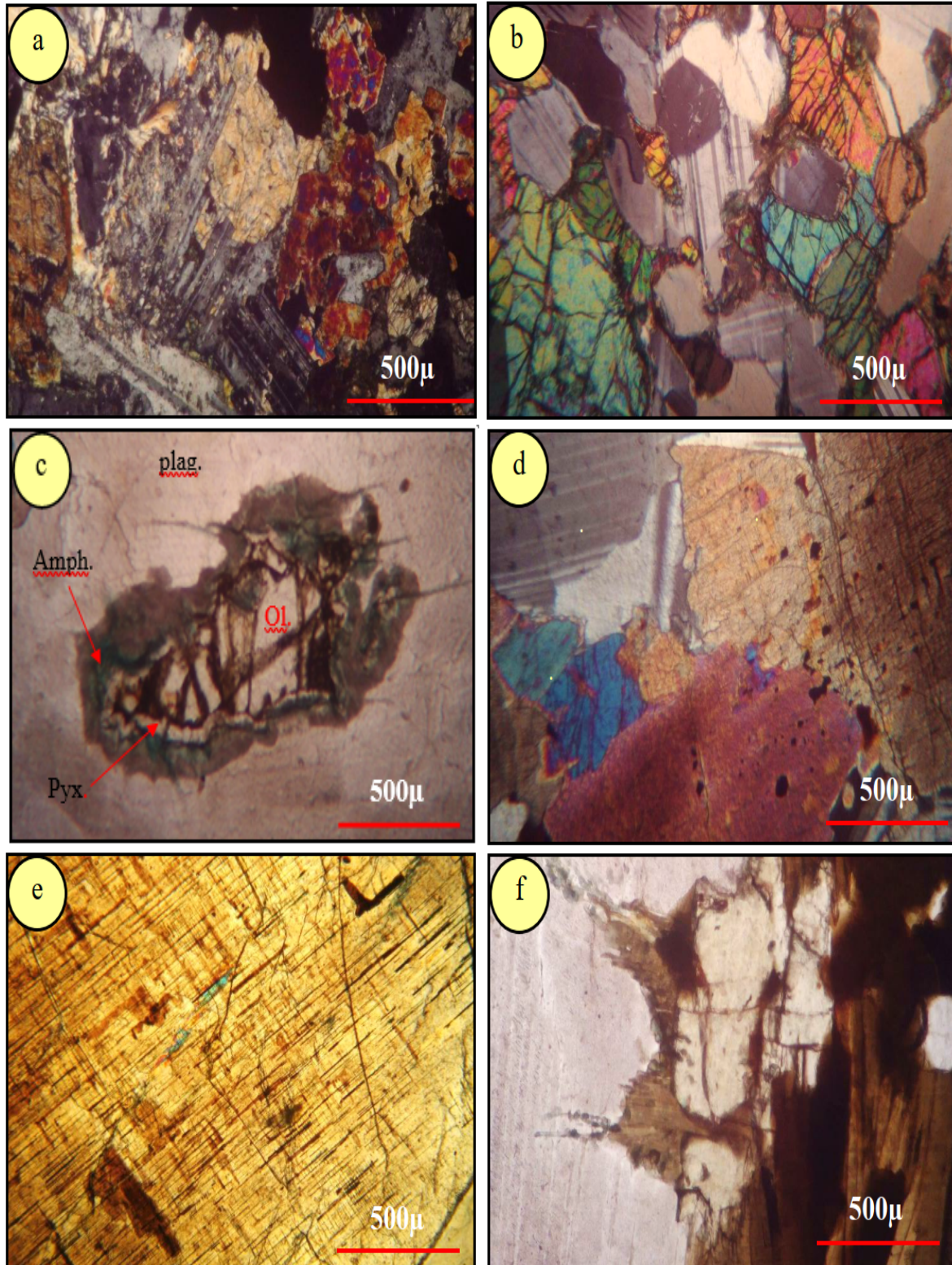


Figure 3. Geological Map of Al-Ahkum area (Modified After [29]).



**Figure 4.** Field description of the gabbroic intrusions. (a.) The basement rocks are covered by the sedimentary rocks (Al-Tawilah Sandstone Group). Al-Maqarirah area, photo looking E. (b.) Gabbroic rocks have sharp contact with older basement rocks. Al-Maqarirah intrusion, photo looking NW. (c.) Gabbroic rocks contain xenoliths of gneiss rocks and crossed by quartz vein, Wadi Al-Ahkum. Photo looking E. (d.) Gabbroic rocks contain xenoliths of amphibolite rocks (Amph.). Al-Maqarirah area, photo looking W. (e.) Gabbroic rocks have massive structure and coarse-grained texture. Al-Maqarirah intrusion, photo looking N. (f.) Gabbroic rocks show weak layered structure. Note the alternating bands of mafic and felsic minerals. Al-Ahkum area, photo looking NW. (g.) Granitic rocks contain xenoliths of gabbroic rocks (Gb.). Al-Ahkum area, photo looking S.



**Figure 5.** Petrography of the gabbroic intrusions (Plate 1) (a.) Normal gabbro from Al-Maqatirah area, C.N. (b.) Olivine gabbro showing intercumulus texture where plagioclase crystal occupied the intergranular spaces between olivine crystals. Al-Ahkum area, C.N. (c.) Kelyphytic structure composed of colorless olivine core (Ol.) surrounded by colorless zone of pyroxene crystals (Pyx.) followed by outer zone of columnar aggregates of green amphibole crystals (Amph.). Olivine gabbro from Al-Ahkum area, C.N. (d.) Olivine-pyroxene gabbro Al-Ahkum area C.N. (e.) Big pyroxene crystal contains small lamellae of orthopyroxene and opaque mineral oriented along the cleavage planes forming exsolution texture. Olivine-pyroxene gabbro from Al-Ahkum area, C.N. (f.) Olivine-biotite gabbro from Al-Maqatirah area. Note that the olivine crystals are mantled by biotite. P.L.

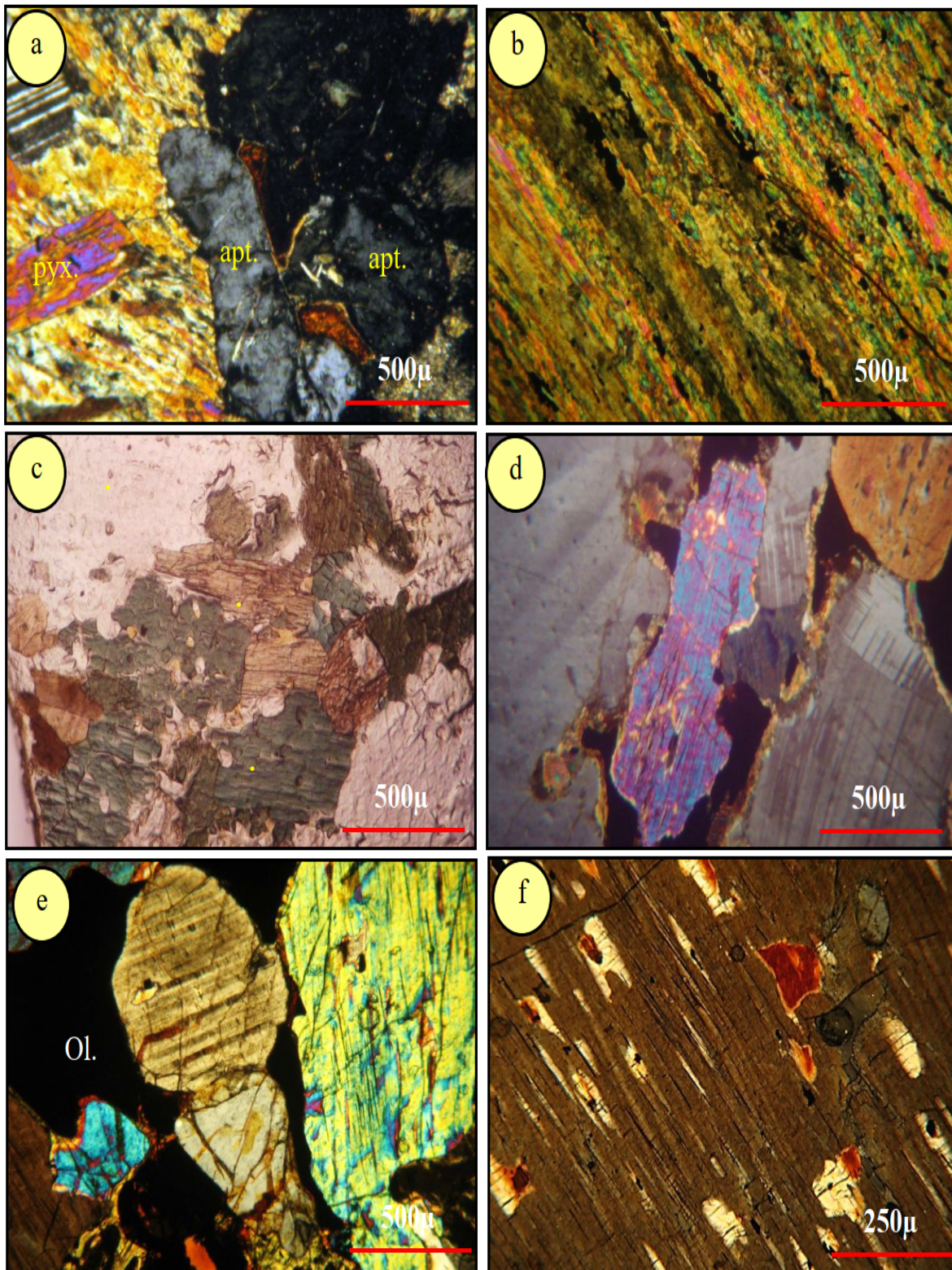


**Figure 6.** Petrography of the gabbroic intrusions (plat 2) (a.) Pyroxene gabbro from Al-Maqatirah area. Note that the pyroxene crystals are severely altered to tremolite-actinolite leaving small fresh relict of pyroxene (pyx.) in the center of some crystals, C.N. (b.) Big pyroxene crystal completely altered to tremolite-actinolite and opaque minerals forming schiller texture. Pyroxene gabbro from Al-Ahkum area, C.N. (c.) Hornblende gabbro from Al-Maqatirah area. Note that the hornblende shows pale green, yellowish green and, yellowish brown colors and some crystals altered to biotite (down left corner), P.L. (d.) Felsic layer composed of plagioclase with few pyroxene and Fe-Ti oxides. Layered gabbro from Al Ahkum area, C.N. (e.) Mafic layer composed of pyroxene, Fe-Ti oxides and olivine with few plagioclase forming cumulus (pyroxene and olivine) and intercumulus (Fe-Ti oxides) textures. Note the reaction rims of phlogopite surrounded the olivine against later formed opaques. Layered gabbro from Al Ahkum area, C.N. (f.) Big pyroxene (augite) crystal contains exsolutions of orthopyroxene (enstatite) crystals and opaque minerals along their cleavage planes. Layered gabbro from Al Ahkum area, C.N.

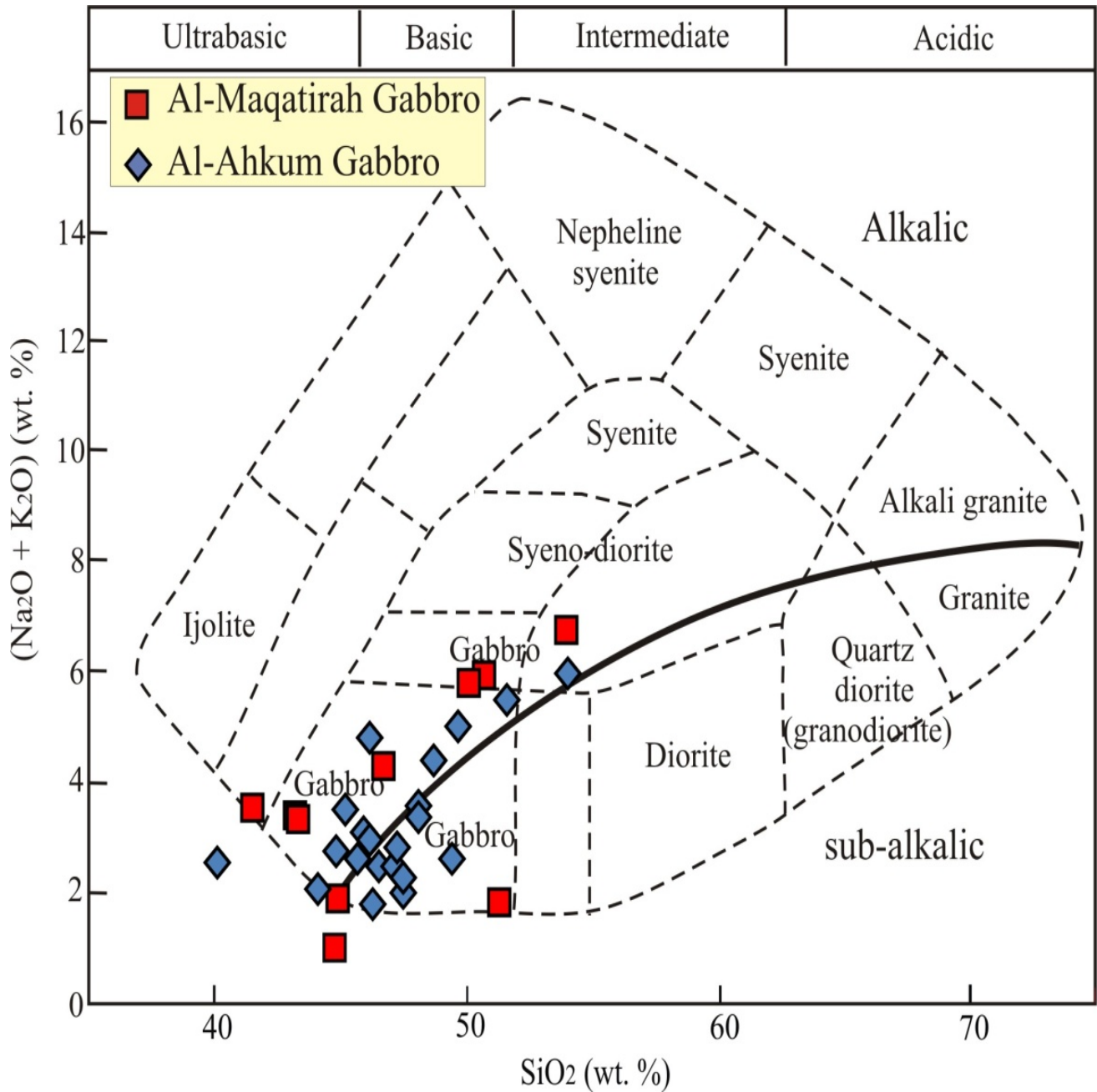


**Figure 7.** Geochemical classification and nomenclature of plutonic rocks using TAS diagram of [39] adopted by [58] for the plutonic rocks. The curved solid line subdivides alkalic from sub-alkalic rocks is after [85].

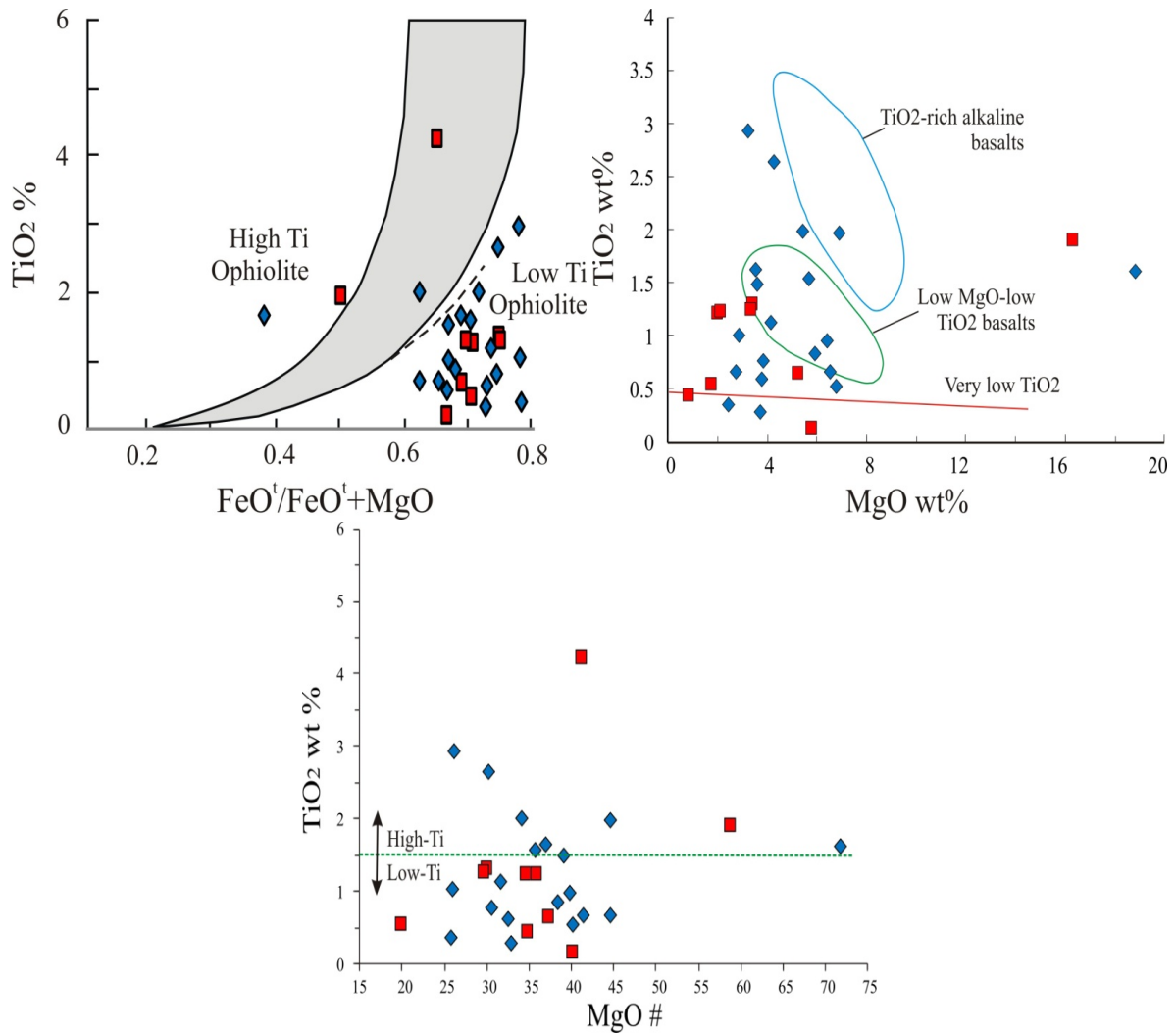


**Figure 8.** (a). TiO<sub>2</sub> vs. FeO<sup>t</sup>/(FeO<sup>t</sup> + MgO) diagram [40] for studied gabbroic rocks. Shaded field denotes gabbroic rocks dredged from Atlantic and Indian Oceans; (b). MgO vs. TiO<sub>2</sub> diagram [41]; and (c) MgO# vs. TiO<sub>2</sub> diagram [42] for studied gabbroic rocks. Symbols as in Fig. 7.

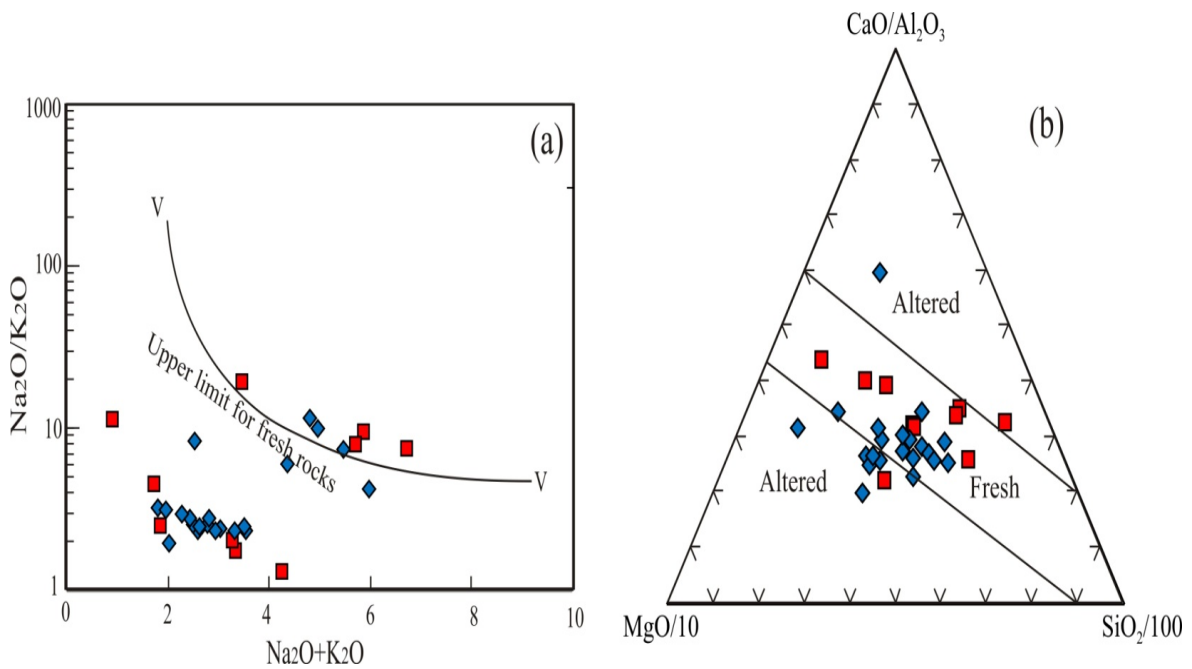


**Figure 9.** (a) Na<sub>2</sub>O/K<sub>2</sub>O vs Na<sub>2</sub>O+K<sub>2</sub>O diagram (after [43]) and (b) CaO/Al<sub>2</sub>O<sub>3</sub>- MgO/10- SiO<sub>2</sub>/100 diagram (after [44]) for the studied gabbroic rocks. Symbols as in Fig. 7.

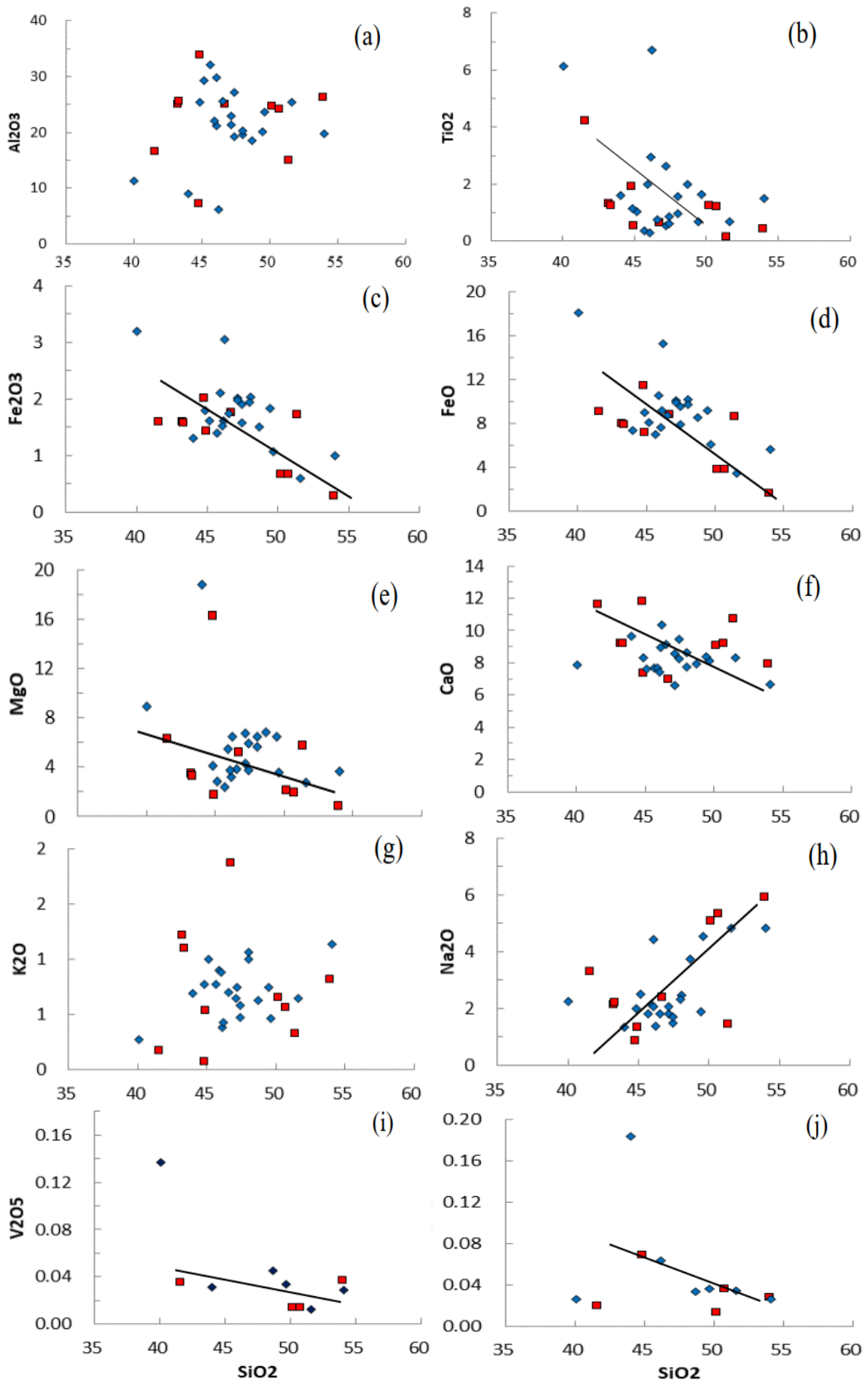


**Figure 10.** Harker diagrams illustrating the whole-rock major element oxides of gabbroic rocks from Al-Maqatirah and Al-Ahkum areas. Symbols as in Fig. 7.

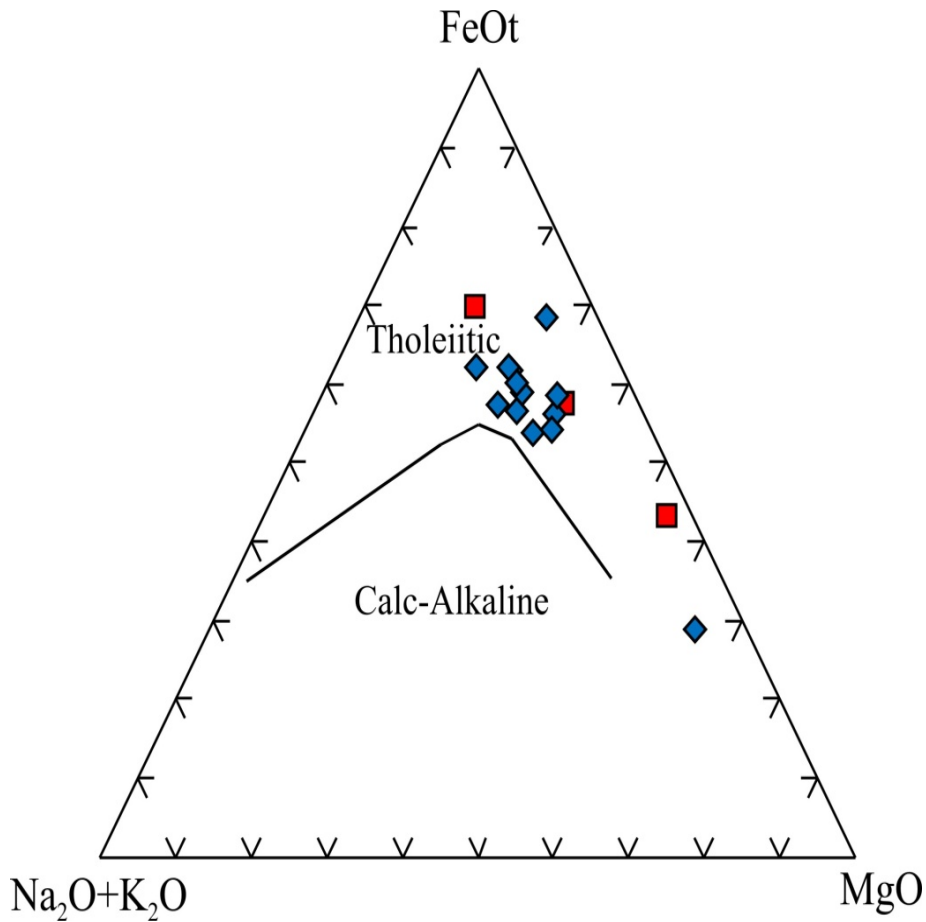


Figure 11. AFM diagram [47] for the studied gabbroic rocks. Symbols as in Fig. 7

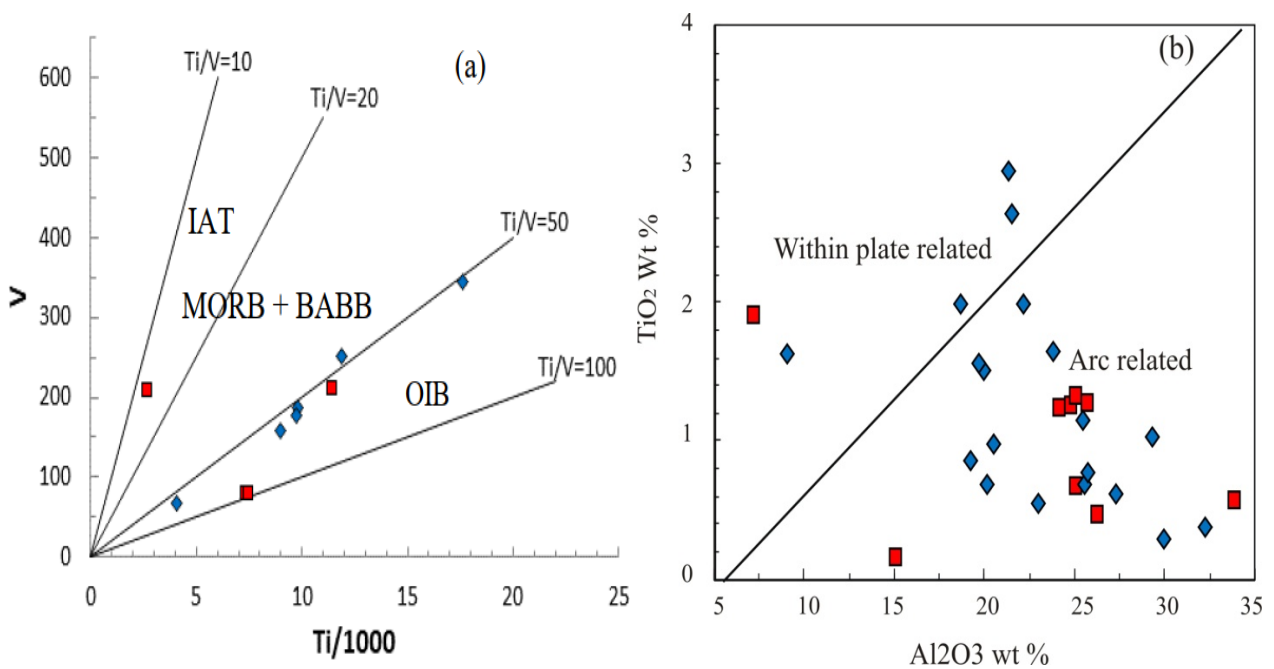


Figure 12. . (a) Ti/1000 vs. V tectonic discrimination diagram [86] for studied gabbroic intrusions from Al-Maqatirah and Al-Ahkum areas. (IAT) island arc tholeiites, (MORB) mid oceanic ridge basalts (BABB) back arc basin basalt and (OIB) ocean island basalt; (b) Al<sub>2</sub>O<sub>3</sub>-TiO<sub>2</sub> diagram for studied gabbroic intrusions from Al-Maqatirah and Al-Ahkum areas [48]. Symbols as in Fig. 7.